University of Alberta

Molecular Simulation of the Wetting of Selected Solvents on Sand and Clay Surfaces

by

Xiao Ni

A thesis submitted to the Faculty of Graduate Studies and Research in partial fulfillment of the requirements for the degree of

Master of Science in Chemical Engineering

Chemical & Materials Engineering

Spring, 2010
Edmonton, Alberta

Examining Committee

Phillip Choi, Chemical and Materials Engineering

Zhenghe Xu, Chemical and Materials Engineering

Tian Tang, Mechanical Engineering

ABSTRACT

Molecular dynamics simulation and density functional theory were applied to calculate heats of immersion (ΔH_{imm}) of *n*-heptane, toluene, pyridine and water on two model sand surfaces and two model clay surfaces. Our results indicated that water showed the highest ΔH_{imm} for the model clay surfaces when multi-molecular water layers were used but the lowest when a single molecular layer was used. Simulations of a single molecular water layer sandwiched between a single molecular layer of the aforementioned organic compounds and the octahedral surface of clay indicated that the water layer was not stable. In particular, water molecules tended to desorb from the surface and clustered together to form water/water hydrogen bonds. Given the nature of bitumen molecules, the current results support the hypothesis that a pre-existing water layer on the sand and clay surfaces in raw oil sands is plausible so long as it is thick enough.

ACKNOWLEDGEMENTS

I would like to thank the following individuals and organizations for their support in completing the project:

Dr. Phillip Choi for his valuable assistance with this project, insightful guidance and encouragement for my academic life, especially those helps when I was puzzled and confused. His unfailing helps really enlightened my thinking.

Centre for Oil Sands Innovation, Alberta Ingenuity and Imperial Oil for the financial support, which made this project possible.

Dr. Xu Wang, Dr. Chunli Li and all the other members in the group. They gave me advice which was really helpful to me academically.

My parents for their permanent supports through my life. Without them, none of my achievements could have been obtained.

The first teacher in my life, my maternal grandmother. And I wish her rest in peace. She established the foundations of my achievements when I was kid. Without her efforts, I could not imagine that I have accomplished so far as an average student.

TABLE OF CONTENTS

LIST OF TABLES

LIST OF FIGURES

Chapter 1

Introduction

1.1 Introduction

Oil sands (tar sands) deposits are widely distributed globally in many continents and countries, such as Africa, Canada, Venezuela, Russia and the United States (Speight, 1991). Alberta's total in-place bitumen reserves amount to 1.7 trillion barrels, and are one of the largest hydrocarbon recourses in the world. More than half of the Alberta oil sands are reserved in the Athabasca area (Speight et al., 1984).

Fast development of Alberta's oil sands is expected to continue, but its pace will depend on successfully meeting a number of challenges. Conventional oil sands extraction process relies on the use of hot water; schematic of the process is shown in Figure 1.1. It resembles the laundry process in which hot water washes off the dirt and stains. However, in the hot water extraction process, hot water separates the bitumen from sand and other minerals. Water extraction is proven to be efficient, but it consumes a lot of water and energy (approximately four barrels of water per barrel of synthetic crude oil produced). Shortage of water resource in the Athabasca area has driven oil sands industries to look for alternative extraction methods (Masliyah, 2009).

Solvent extraction may be a solution to these problems. The target organic solvent should satisfy economic, environmental, and technical requirements; a suitable solvent should also have low affinity for the mineral surfaces to have easy solvent recovery and the ability to lower the viscosity of bitumen.

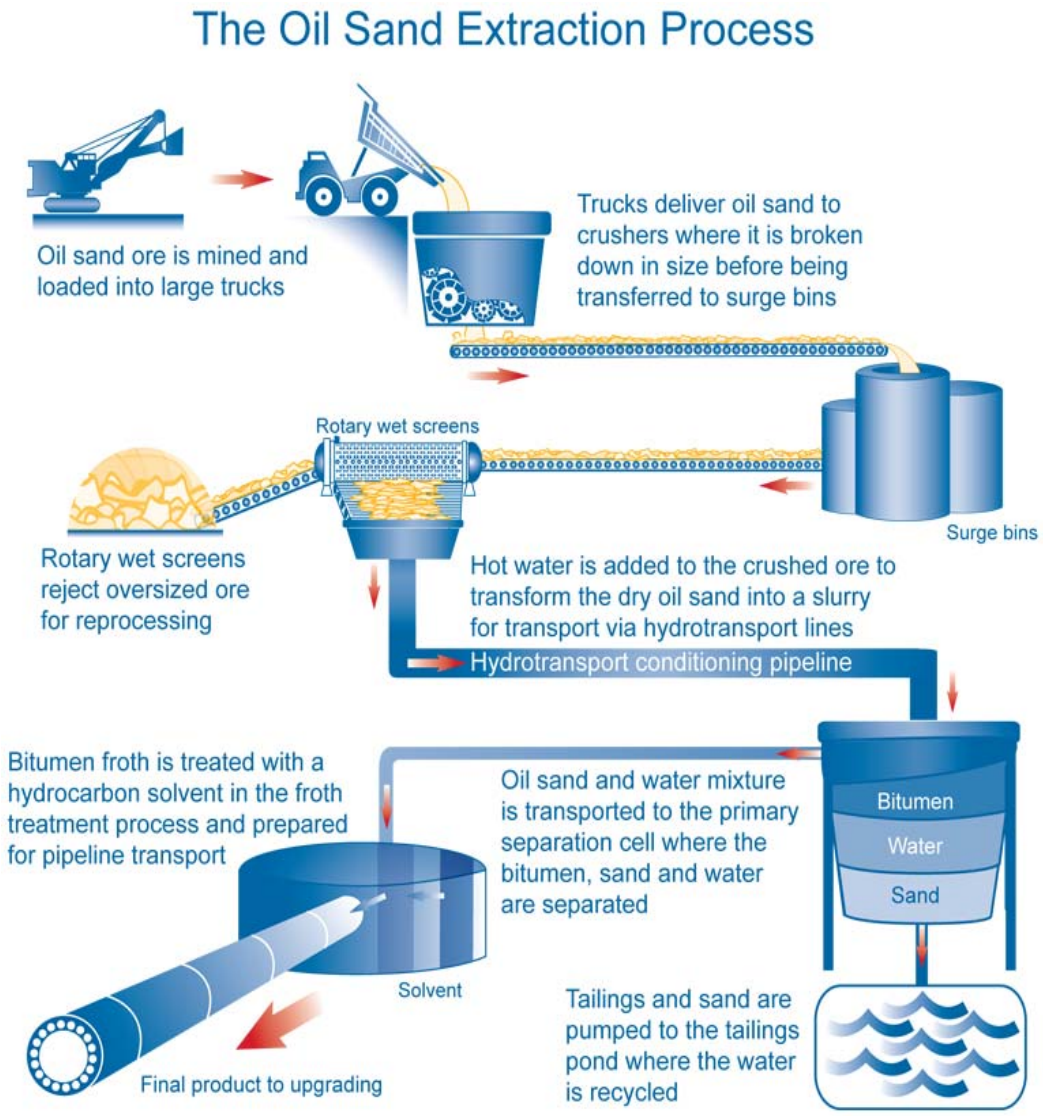

Figure 1.1 Schematic of Oil Sands Water Extraction Process (hatch.ca 2008)

1.2 Interfacial Behavior

An interface is a surface forming the boundary between two different phases, such as two immiscible liquids or an insoluble solid and a liquid. Interface is the place where two types of immiscible molecules or chemical structures can interact chemically and/or physically with each other. Great attention has been paid to the interfacial science. Materials with unique surface properties and specifically modified surface materials were investigated and studied widely (Calderon et al., 2008; Al Othman and Apblett, 2009; Sun et al., 2009).

Interfacial behavior also plays an important role in mineral processing (the practice of beneficiating valuable minerals form their ores) (Grundl and Sparks, 1999; De Leeuw et al., 2001). The oil sands industry is not an exemption; surface/interface chemistry leads to some extraordinary phenomena we observed in the extraction process (Masliyah et al., 2004). Obviously, such knowledge will help optimize the water extraction process and may lead to innovative methods for bitumen liberation.

1.3 Purpose of the Project

Major objective of this work is to study the affinities of selected liquids (including aliphatic and aromatic solvents and water) for model sand and clay surfaces by using molecular dynamics (MD) simulation. Possible factors that would influence the heat of immersion of the aforementioned liquids will be further studied. It is expected that these results would provide insights needed to come up with a solvent used in the extraction process.

It is believed that a water layer exists on the mineral surfaces of interest (Chapter 2), stability of such water layers with different thicknesses on a model surface was investigated as this would affect the choice of solvent. In particular, the behavior of water layers with different thicknesses and with the organic molecules was also studied.

1.4 Structure of this Thesis

This thesis consists of six chapters. The chemistry of oil sands is described briefly in Chapter two; characteristics of the clay and silica surfaces will also be presented. Chapter three presents a review on the computer simulation methods used in the present work. Results of MD calculations of the heats of immersion of the selected liquids on four different model surfaces will be reported in Chapter four. Possible factors affecting heat of immersion will be discussed in this chapter as well. In Chapter five, simulation results of water layers with different thicknesses on model clay surfaces will be presented; behavior of water layer and organic layer on the octahedral surface was also studied. Important findings of this project and recommendations for the future work are summarized in Chapter six.

1.5 References

Al Othman, Z., Apblett, A. W. (2009) Synthesis of Mesoporous Silica Grafted with 3-glycidoxypropyltrimethoxy-silane, *Materials Letters*, 63, 27, 2331-2334

Calderon, J. U., Lennox, B, Kamal, M. R. (2008) Thermally Stable Phosphonium-Montmorillonite Organoclays, *Applied Clay Science*, 40, 1-4, 90-98

De Leeuw, N. H., Redfern, S. E., Cooke, D. J., Osguthorpe, D. J., Parker, S. C. (2001) Modeling Dynamics Properties of Mineral Surfaces, *ACS Symposium Series*, 789, 97-112

Grundl, T. J., Sparks, D. L. (1999) Kinetics and Mechanisms of Reactions at the Mineral-Water Interface: An Overview, *ACS Symposium Series*, 715, 2-11

Hatch Corporate Website (2008), *The Hatch Report*, http://www.hatch.ca/about_us/hr_july2008/fort_hills_phase_ii.html

Masliyah, J., Zhou, Z., Xu, Z., Czarnecki, J., Hamza, H. (2004) Understanding Water-Based Bitumen Extraction from Athabasca Oil Sands, *Canadian Journal of Chemical Engineering*, 82, 628-654

Masliyah, J. (2009) Course Notes of Ch E 534: Fundamentals of Oil Sands Extraction Winter, 2009, University of Alberta, AB

Speight, J. G., Long, R. B., Trowbridge, T. D. (1984) Factors Influencing the Separation of Asphaltenes from Heaving Petroleum Feedstocks, *Fuel*, 63, 616-620

Speight, J. G. (1991) *The Chemistry and Technology of Petroleum*, 2nd ed., Marcel Dekker, New York, NY

Sun, F., Pan, Y., Wang, J., Wang, Z., Hu, C., Dong, Q. (2009) Preparation of Conducting Polyaniline and Polyaniline-Fluorinated Momtmorillonite nanocomposites in Supercritical Carbon dioxide, *Journal of Macromolecular Science, Part A: Pure and Applied Chemistry*, 46, 1, 37-45

Chapter 2

Oil Sands

2.1 Oil Sands Chemistry

Oil sands are composed of bitumen, solid minerals, water, and some dissolved salts. They tend not to have an exact concentration of each component. The composition of the bitumen and water is approximately 16 wt% and 5 wt%, respectively (Wallace et al., 2004; Masliyah, 2009); the balance constitutes the solid minerals content.

Athabasca bitumen is thought as the products of the biodegradation, only the molecules with long chain and/or high aromaticity were left during this process. The components in bitumen can be summarized in the phrase "SARA", which stands for "Saturates, Aromatics, Resins, Asphaltenes". Woods et al. (2008) studied several samples of typical Alberta bitumen and found that it has 16-17% saturates, 37% resins, 18-21% asphaltenes and 25-29% aromatics.

Aromatic rings not only exist in the aromatic fraction of the bitumen; pyrolysis experiments support the idea that they are also the fundamental units of aspahltene molecules (Peng et al., 1997; Gray, 2003). The molecular structure of asphaltene is unknown, but some attempts of building asphaltene model structures by using Monte Carlo methods were already made; the building blocks were mainly short chains and small aromatic rings including heterocyclic rings (Sheremata et al., 2004). Due to the limitation of computation resource and uncertainty in the structures of molecules in bitumen, the interaction between

bitumen and mineral surfaces cannot be obtained from calculations currently. However, the interactions between aromatics and inorganic surfaces are easy to be investigated. These calculations may be very helpful in understanding the bitumen behavior in the extraction process.

Two aromatic solvents, toluene and pyridine (heterocyclic solvent), were chosen as our model solvents. Toluene is widely used in the bitumen related experiments and a very good solvent for bitumen (Masliyah, 2009; Acevedo et al., 2002). Since part of the sulfur and oxygen, most of nitrogen and metal in the bitumen are presented in the heterocyclic rings (Gray, 2009); pyridine was chosen as another model aromatic solvent in our simulations. Toluene and pyridine were both used as building units for studying asphaltene in simulations previously (Peng et al., 1997; Sheremata et al., 2004).

As aliphatic components also exist in the bitumen, alkane, in particular, *n*-Heptane was used in our simulations. Like toluene, *n*-Heptane is commonly used in the bitumen experiments (Tarkan et al., 2009).

2.2 Water and Electrolytes

The most important characteristic of mineral surfaces encountered in oil sands is hydrophilic. It is the hydrophilic nature of sand grains in oil sands ores that makes Alberta oil sands processable (Mossop, 1980). One hypothesis indicates that there may be a thin layer of water on the mineral surfaces leading to the hydrophilic nature of the mineral surface. Where the water resided in the oil sand ore is still a topic of controversy. In the 30's and 40's of the last century, some researchers

postulated that minerals in oil sands may be enveloped by a thin layer of water (Clark, 1944). A schematic is presented to show that the water forms a thin film that partially covers or totally envelops the sand grain surfaces (Figure 2.1). The thickness of this thin water layer on the mineral surfaces has been speculated to be approximately 10 nm (Takamura, 1982). An NMR study of oil sands by Sobol et al. (1985) demonstrated that there exist two types of water; one forms the bridge between sand grains and the other appears on the sand or clay mineral surfaces. But a contrary point of view was concluded by Zajic et al. (1981), no evidence of water layer was found from their transmission electron microscopy experiments. Recently, Czarnecki et al. (2005) conducted some calculations of Young-Laplace equation of capillarity to study the stability of the water layers with different thicknesses on quartz surface. Based on their results, it is likely a water layer of 2 nm (20 Å) could be stable under neutral pH.

The dissolved ions and natural surfactants existed in this "connate" water of oil sands ore, which could affect the processability in extraction process (Masliyah et al., 2004).

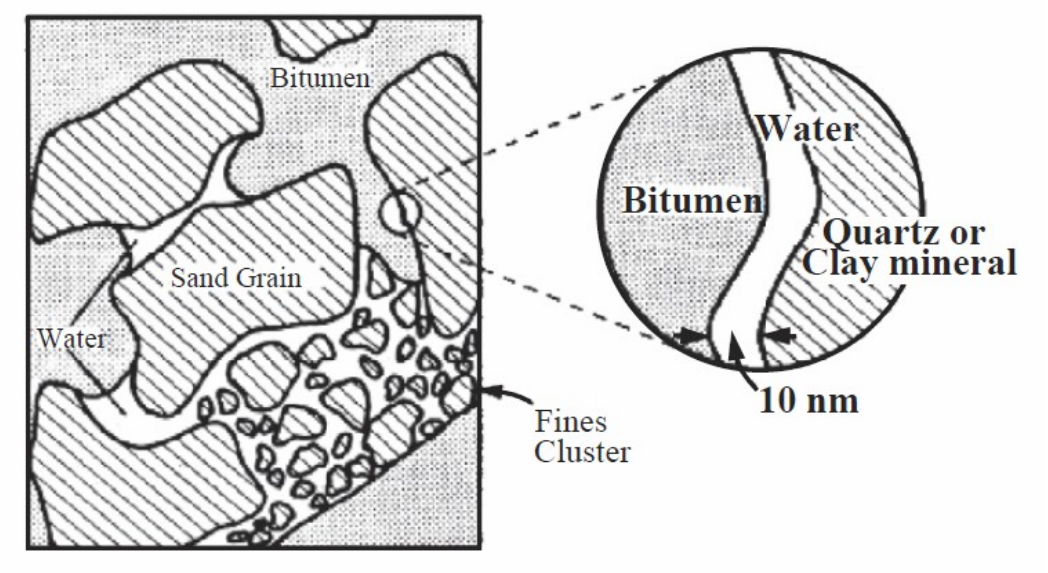

Figure 2.1 Structural Model of the Athabasca Oil Sands (Takamura, 1982)

2.3 Sand

Majority of the solid minerals in oil sands is quartz (up to 82%) (Hepler and Smith, 1994). Crystalline silica (SiO_2) exists in many polymorphic forms, while alpha-quartz is one of the most common polymorphs (Konecny, 2001). Cristobalite is another polymorph of silica, which chemical and physical properties is different from the quatz (Humphrey and King, 1952).

It is found that natural sand surface has hydroxyl groups that are formed from the strained Si—O—Si structure and moisture; removal of surface hydroxyl groups is occurred slowly only at high temperatures (Zhdanov 1987; Zhuravlev et al., 2001). There are two types of the silanols groups, vicinal and geminal. For the vicinal group, each one hydroxyl group is connected to the silicon atom while the geminal type, two hydroxyl groups can be attached on one silicon atom. NMR experiments of silica contacted with water vapor done by Chuang and Maciel

(1997) indicated that only 6% of the total silanol groups are geminal. The infra-red results also showed that very few germinal hydroxyls can be found on the fully hydrated surface (Hockey and Pethica, 1961). These surface hydroxyl groups could react with adjacent water and organic molecules, especially the polar species like alcohols (Kellum and Smith, 1967). Our silica surface models were both hydroxylated. The interface or surface behavior of silica surface like wettablity can be modified by the reaction on these surface hydroxyl groups. For example, Yamaguchi (2005) used ionic liquid-modified silica as a heterogeneous epoxidation catalyst. The surface hydroxyl groups also increase the electrostatic interaction, because the OH group can be seen as donor/accepter of protons (Hassanali and Singer, 2007). The existence of surface hydroxyl groups also affects the heat of immersion value. Takei and Chikazawa (1998) found that not only the density of surface hydroxyl groups can contribute to the increasing affinity of silica surfaces, also the configuration of the hydroxyl groups.

2.4 Clay

Clay is one of the most abundant minerals on our planet, and it is one of the earliest mineral material humankind used. The space between repeating layers and various adsorbing sites on the basal surfaces of these layers make it a good sorbent. In industry and academic, clay is commonly used as sorbent removing hazardous heavy metal ions and organic contaminants in processing polluted soils or wastewater (Dable et al., 2008). Some researches suggest that the metal cations

in clay can also exchanged with the toxic ions (Oladoja and Ademoroti, 2006). The organic modified clay behaves differently in the adsorption process.

Clays only consist of a small weight percentage of the total oil sands ore and only appear as fines in the ore, but they are considered as problematic in the conventional hot water extraction process (Masliyah, 2009). Some studies have shown that clay can stay on the air bubble surface, and inhibits the air bubble contact with the liberated bitumen droplets; also in the froth treatment, the clay minerals cannot be easily removed to purify the liberated bitumen (Tu, 2004; Liu et al., 2005).

Kaolinite was chosen as our clay model since it is the most abundant clay minerals encountered in oil sands (Masliyah, 2009). It is non-porous and non-swelling (Tunega et al., 2002a). Kaolinite has a layered structure and each repeating layer has two basal surfaces—octahedral and tetrahedral surfaces, also known as the alumina surface and silica surface because of the types of atoms located on these surfaces (See Figure 2.2). The repeating layers are stacked together by the interlayer electrostatic forces, usually hydrogen bonds (Murashov and Demchuk, 2005). Both surfaces have adsorption sites, especially for the octahedral surface, interacting strongly with water or polar organic molecules, as demonstrated by Tunega et al. (2002b).

Besides these two basal surfaces, the characteristics of the edges are not quite clear right now, but according to Croteau et al. (2009), water and organic solvents show the highest affinity for the edges. Balard et al. (1997) found that the

basal surfaces and lateral surfaces (edge) in the kaolinite structure give this mineral heterogeneity character.

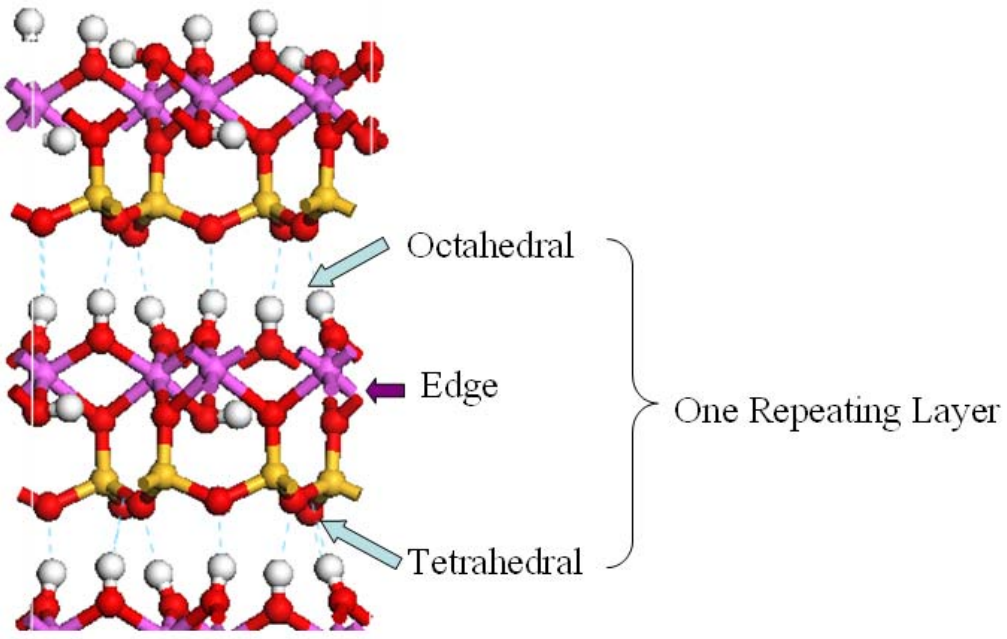

Figure 2.2 Structure of the Kaolinite (Broken Line—Hydrogen Bonds; Red—Oxygen; White—Hydrogen; Purple—Aluminum; Yellow—Silicon)

2.5 Surface Behavior

Surface behavior plays a significant role not only in the bitumen extraction, but also in many other scientific and industrial applications. Some researchers have shown long time ago that surfactants which are able to adsorb on the interface could change the wetting behavior of clay dramatically (Jada and Debih 2009). Meanwhile, the surface functional groups (polar groups, charged groups, etc.) could help the surface raise its affinity for water (Takei and Chikazawa., 1998). Jouany and Chassin (1987) measured the surface energy of organo-mineral

complexes to evaluate the contribution of adsorbed organic compounds to changing clay surface properties.

2.5.1 Heat of immersion

Heat of immersion, also known as enthalpy of wetting or immersion enthalpy, is used to quantify the affinity of fluids for a surface. It is defined as the difference (at a fixed temperature) between the energy of a solid completely immersed in a wetting liquid, and those of the solid and liquid taken separately (Dekany et al., 1984). The free energy of immersion and heat of immersion can be defined thermodynamically in equations (2-1) and (2-2) as follows (Douillard et al., 1995):

$$\Delta G_{imm=}\gamma_{SL}-\gamma_S \quad (2\text{-}1)$$

$$-\Delta H_{imm}=\gamma_S-\gamma_{SL}-T[\partial(\gamma_S-\gamma_{SL})/\partial T]_P \quad (2\text{-}2)$$

Experimental measurement of the heat of immersion is done based on equation (2-2) (Mlandrini et al., 1997).

2.5.2 Wettability of Surface

Wetting phenomena refer to the behavior of liquid on the surface of interest; wettability of surfaces has significant impact on the flotation, and other separation processes. One common expression of wettability of a solid surface is quantified by the contact angle θ defined in the Young's equation (Young, 1805), which relates the three phase contact angle of a liquid droplet on a planar substrate to the surface tensions of the three interfaces involved:

$$\gamma_{lv}\cos\theta=(\gamma_{sv}-\gamma_{sl}) \quad (2\text{-}3)$$

where γ_{ab} represents the surface tension of the a-b interface with a and b could be either vapor (v), liquid (l), or solid (s). Some attempts of using MD simulation to obtain contact angles were done (Hautman and Klein, 1991; Nielsen et al., 2005).The smaller the contact angle, the stronger the affinity of the liquid for the solid surface. One extreme case is that the contact angle is close to zero which means that the liquid can wet the surface totally.

It is believed that the substrate structure and composition strongly affects the interfacial behavior (Wang et al., 2009). Hautman and Klein (1991) used MD simulation to investigate wetting behavior of 90 water molecules on an alkane crystal surface (hydrophobic) on a microscopic length level; they found that water molecules form a cluster on the alkane surface, when the surface was terminated with hydroxyl groups, water molecules would spread out more over the surface.

2.6 References

Acevedo, S., Ranaudo, M. A., Garcia, C., Castillo, J., Fernandez, A. (2003) Adsorption of Asphaltenes at the Toluene-Silica Interface: A Kinetic Study, *Energy & Fuels*, 17, 2, 257-261

Balard, H., Saada, A., Papirer, E., Siffert, B. (1997) Energetic Surface Heterogeneity of Illites and Kaolinites, *Langmuir*, 13, 1256-1259

Chuang, I. S., Maciel, G. E. (1997) A Detailed Model of Local Structure and Silanol Hydrogen Bondings of Silica Gel Surfaces, *Journal of Physical Chemistry B*, 101, 16, 3052-3064

Clark, K. A. (1944) Hot-Water Separation of Alberta Bituminous Sand, *Canadian Institute of Mining and Metallurgy-Transactions*, 47, 521-523

Croteau, T., Bertram A. K., Patey, G. N. (2009) Simulation of Water Adsorption on Kaolinite under Atmospheric Conditions, *Journal of Physical Chemistry A*, 113, 7826-7833

Czarnecki, J., Radoev, B., Schramm, L. L., Slavchev, R. (2005) On the Nature of Athabasca Oil Sands, *Advances in Colloid and Interface Science*, 114-115, 53-60

Dable, P. J. M. R., Adjoumani, Y. J., Yao, B., Ado, G. (2008) Wastewater Dephosphorization Using Crude Clays, *International Journal of Environmental Science and Technology*, 5, 1, 35-42

Dekany, I., Szanto, F., Nagy, L. G. (1984) Sorption and Immersional Wetting on Clay Minerals Having Modified Surface, *Journal of Colloid and Interface Science*, 103, 2, 321-331

Douillard, J. M., Zoungrana, T., Partyka, S. (1995) Surface Gibbs Free Energy of Minerals: Some Values, *Journal of Petroleum Science and Engineering*, 14, 51-57

Gray, M. R. (2003) Consistency of Asphaltene Chemical Structures with Pyrolysis and Coking Behavior, *Energy & Fuels*, 17, 1566-1569

Gray, M. R. (2009) Course Notes of ChE522: Fundamentals of Oil Sands Upgrading Winter, 2009, University of Alberta, AB

Hassanali, A. A., Singer, S. J. (2007) Model for the Water-Amorphous Silica Interface: the Undissociated Surface, *Journal of Physical Chemistry B*, 111, 11181-11193

Hepler, L. G., Smith, R. G. (1994) the Alberta Oil Sands: Industrial Procedures for Extraction and Some Recent Fundamental Research, *AOSTRA Technical Publication*, 14

Hockey, J. A., Pethica B. A. (1961) Surface Hydration of Silicas, *Transactions of the Faraday Society*, 2247-2262

Humphrey, G. L., King, E. G. (1952) Heats of Formation of Quartz and Cristobalite, *Journal of American Chemical Society*, 74, 8, 2041-2042

Hautman, J. and Klein, M. L., (1991) Microscopic Wetting Phenomena, *Physical Review Letters*, 67, 13, 1763-1766

Jada, A., Debih, H. (2009) Hydrophobation of Clay Particles by Asphaltenes Adsorption, *Composite Interfaces*, 16, 219-235

Jouany, C., Chassin, P., (1987) Determination of the Surface Energy of Clay-Organic Complexes by Contact Angle Measurements, *Colloids and Surfaces*, 27, 289-303

Kellum, G. E., Smith R. C. (1967) Determination of Water, Silanol, and Strained Siloxane on Silica Surfaces, *Analytical Chemistry*, 39, 3, 341-345

Konecny, R. (2001) Reactivity of Hydroxyl Radicals on Hydroxylated Quartz Surface. 1. Cluster Model Calculations, *Journal of Physical Chemistry B*, 105, 6221-6226

Liu J., Xu Z., Masliyah, J. (2005) Interaction Forces in Bitumen Extraction from Oil Sands, *Journal of Colloid and Interface Science*, 287, 507-520

Malandrini, H., Sarraf, R., Faucompre, B., Partyka, S., Douillard, J. M. (1997) Characterization of Quartz Particle Surfaces by Immersion Calorimetry, *Langmuir*, 13, 1337-1341

Masliyah, J., Zhou, Z., Xu, Z., Czarnecki, J., Hamza, H. (2004) Understanding Water-Based Bitumen Extraction from Athabasca Oil Sands, *Canadian Journal of Chemical Engineering*, 82, 628-654

Masliyah, J. (2009) Course Notes of ChE 534: Fundamentals of Oil Sands Extraction Winter, 2009, University of Alberta, AB

Mossop, G. D. (1980) Geology of the Athabasca Oil Sands, *Science*, 207, 145-152

Murashov, V. V., Demchuk, E. (2005) A Comparative Study of Unrelaxed Surfaces on Quartz and Kaolinite, Using the Periodic Density Functional Theory, *Journal of Physical Chemistry B*, 109, 10835-10841

Nielsen, S. O., Srinivas, G., Lopez C. F., Klein, M. L., (2005) Incorporating a Hydrophobic Solid into a Coarse Grain Liquid Framework: Graphite in an Aqueous Amphiphilic Environment, *Journal of Chemical Physics*, 123, 124907

Oladoja, N. A., Ademoroti, C. M. A. (2006) the Use of Fortified Soil-Clay as On-site System for Domestic Wastewater Purification, *Water Research*, 40, 613-620

Peng P., Morales-Izquierdo, A., Hogg, A., Strausz, O. P. (1997) Molecular Structure of Athabasca Asphaltene: Sulfide, Ether, and Ester Linkages, *Energy & Fuel*, 11, 1171-1187

Sheremata, J. M., Gray, M. R., Dettman, H. D., McCaffrey, W. C. (2004) Quantitative Molecular Representation and Sequential Optimization of Athabasca Asphaltenes, *Energy & Fuels*, 18, 1377-1384

Sobol, W. T., Schreiner, L. J., Miljkovic, L, Marcondes-Helene, M. E., Reeves, L. W., Pintar, M. M. (1985) NMR Line Shape-Relaxation Correlation Analysis of Bitumen and Oil Sands, *Fuel*, 64, 583-590

Takamura, K., Chow, R. S. (1982) Microscopic Structure of Athabasca Oil Sands, *Canadian Journal of Chemical Engineering*, 60, 538-545

Takei, T., Chikazawa, M. (1998) Origin of Differences in Heats of Immersion of Silicas in Water, *Journal of Colloid and Interface Science*, 208, 570-574

Tarkan, H. M., Bayliss, D. K., Finch, J. A. (2009) Investigation on Foaming Properties of Some Organics for Oily Bubble Bitumen Flotation, *International Journal of Mineral Processing*, 90, 1-4, 90-96

Tunega, D., Benco, L., Haberhauer, G., Gerzabek, M. H., Lischka, H. (2002a) *Ab Initio* Molecular Dynamics Study of Adsorption Sites on the (001) Surfaces of 1:1Dioctahedral Clay Minerals, *Journal of Physical Chemistry B*, 106, 11515-11525

Tunega, D., Haberhauer, G., Gerzabek, M. H., Lischka, H. (2002b) Theoretical Study of Adsorption Sites on the (001) Surfaces of 1:1 Clay Minerals, *Langmuir*, 18, 139-147

Tu, Y., Li Z., Pleizier, G., Ng, S., Chung, K. H. (2004) Separation and Characterisation of Problematic Solids from Athabasca Oil Sands and Waste Units Samples, *Canadian Journal of Chemical Engineering*, 82, 678-686

Wang, J., Kalinichev, A. G., Kirkpatrick, R. J. (2009) Asymmetric Hydrogen Bonding and Orientational Ordering of Water at Hydrophobic and Hydrophilic

Surfaces: A Comparison of Water/Vapor, Water/Talc, and Water/Mica Interfaces, *Journal of Physical Chemistry C*, 113, 11077-11085

Woods, J., Kung, J., Kingston, D., Kotlyar, L., Sparks, B., McCracken, T. (2008) Canadian Crudes: A Comparative Study of SARA Fractions from a Modified HPLC Separation Technique, *Oil & Gas Science and Technology*, 63, 1, 151-163

Yamaguchi, K., Yoshida, C., Uchida, S., Mizuno, N. (2005) Peroxotungstate Immobilized on Ionic Liquid-Modified Silica as a Heterogeneous Epoxidation Catalyst with Hydrogen Peroxide, *Journal of American Chemical Society*, 127, 2, 530-531

Young, T. (1805) an Essay on the Cohesion of the Fluids, *Philosophical Transactions: Royal Society (London)*, 95, 65-87

Zajic, J. E., Cooper, D. G., Marshall, J. A., Gerson, D. F. (1981) Microstructure of Athabasca Bituminous Sand by Freeze-Fracture Preparation and Transmission of Electron Microscopy, *Fuel*, 60, 7, 619-623

Zhdanov S. P. (1987) IR Study of Hydroxylated Silica, *Langmuir*, 3, 960-967

Zhuravlev, N. D., Siepmann, J. I., Schure, M. R. (2001) Surface Coverages of Bonded-Phase Ligands on Silica: A computational Study, *Analytical Chemistry*, 73, 4006-4011

Chapter 3

Molecular Simulation & its Applications

3.1 Molecular Dynamics (MD) Simulation

Computer has been one of the most fascinating and powerful inventions for the past few decades. The first intent of such an electronic computing machine is to do a huge amount of repeating calculations at a speed we never had; based on that benefit, computer simulation has made our way to model materials on a molecular level. Rapid development of hardware is making simulation faster, cheaper, and possible on almost any personal computer. And many computer languages and techniques have been developed to do various jobs.

Fundamentals of molecular simulation are based on the knowledge of statistical mechanics, and it uses many approximations to solve the problems which may not be exactly solvable. In many cases, simulation results can offer detailed information about a system that is difficult to obtain experimentally. There are two types of classical molecular simulations available: molecular dynamics (MD) and Monte Carlo (MC) simulations. In these two types of simulations, system setups are similar including the application of classical force fields, and employment of periodic boundary conditions. In MC simulation, acceptance of a new configuration is determined by the Metropolis sampling algorithm. And average structure and properties can be obtained from these configurations. In MD simulation, the Newtonian mechanics is applied to generate new configurations of atoms in the system, ensemble averages were

obtained by averaging over a long trajectory (Allen and Tildesley, 1991; Jorgensen and Tirado-Rives, 1996).

The concept of ensemble is described as many individual microscopic configurations of a very large system that yield the same macroscopic properties. Statistical ensembles are commonly determined by fixed thermodynamic variables such as E (energy); T (temperature); V (volume); N (number of particles) or μ (chemical potential). One basic ensemble is called NVE or microcanonical ensemble; some calculation methods of other ensembles such as NVT were developed from microcanonical ensemble. Hamiltonian mechanics can be used to obtain microcanonical ensembles (Tuckerman and Martyna, 2000). Consider N particles in the system under the influence of the internal forces, the system is determined by Newton's second law

$$m_i\ddot{\mathbf{r}}_i=\mathbf{F}_i \tag{3-1}$$

$\mathbf{r}_i$ and m_i are the spatial positions and masses of particles, while $\mathbf{F}_i$ are the forces imposed on them. $\mathbf{F}_i$ can be derived from Eq. 3-2

$$\mathbf{F}_i = -\frac{\partial U}{\partial \mathbf{r}_i} \tag{3-2}$$

where $U(\mathbf{r}_1 \cdot \cdots \mathbf{r}_N)$ and is the interparticle potential. The Newton's equation can be expressed in the Hamiltonian form as follows:

$$H(\mathbf{p},\mathbf{r}) \equiv H(\mathbf{p}_1, \ldots, \mathbf{p}_N, \mathbf{r}_1, \ldots, \mathbf{r}_N) = \sum_{i=1}^{N} \frac{\mathbf{p}_i^2}{2m_i} + U(\mathbf{r}_1, \ldots, \mathbf{r}_N) \tag{3-3}$$

where $\mathbf{p}_1 \cdot \cdots \mathbf{p}_N$ are momenta of the particles.

Since all forces experienced by the particles are conservative, the system energy is constant as shown in the following equation:

$$H(\mathbf{p},\mathbf{r})=E \tag{3-4}$$

Limitations of the *NVE* ensemble is obvious, microcanonical conditions are not consistent with many experimental conditions such as constant temperature and volume. One of the approaches is using non-Hamiltonian mechanics to generate either *NVT* or *NPT* ensemble in which the energy of the system can fluctuate.

The idea of developing the dynamical ensemble came from Andersen (1980). Under constant temperature, the energy of a system with N particles should fluctuate and the velocities of particles in the system should be in consistence with the Maxwell-Boltzman distribution at that temperature. To achieve this objective, stochastic forces were employed into the system modifying the kinetic energy of the system throughout the simulation. This method (Roy, 2008) can be considered as introducing a heat bath connected to the system, where the particles in the bath collide with the particles in the system to rescale the velocities (Figure 3.1).

In *NVT* simulations, momentum changes associated with particles is supplemented by a stochastic collision term $d\mathbf{p}_i/dt$ for using as equations of motion. When each collision occurs, the momentum of one particle is changed instantaneously. During the simulation, the time between collisions occurred to a particular particle happens in accordance with a Poisson process. For a liquid subjected to a fixed volume, the collision rate per particle is suggested as

$$C_{rate}=\lambda_T/\rho^{1/3}\mathrm{N}^{1/3} \tag{3-5}$$

where λ_T and ρ is the thermal conductivity and density of the liquid, N is the number of particles in the system. After the collision, the momentum of the particle is chosen randomly from the Boltzmann distribution at temperature T. Between stochastic collisions, the atoms in the system is still microcanonical, evolving without the stochastic term. This method leads to a *NVT* ensemble (Parzen, 1962).

Due to calculation limit, finite sized cell has to be used. Therefore, periodic boundary conditions are used in computation. The finite system is replicated infinitely throughout the space to mimic bulk system or two dimensional infinite systems (Ballenegger et al., 2000).

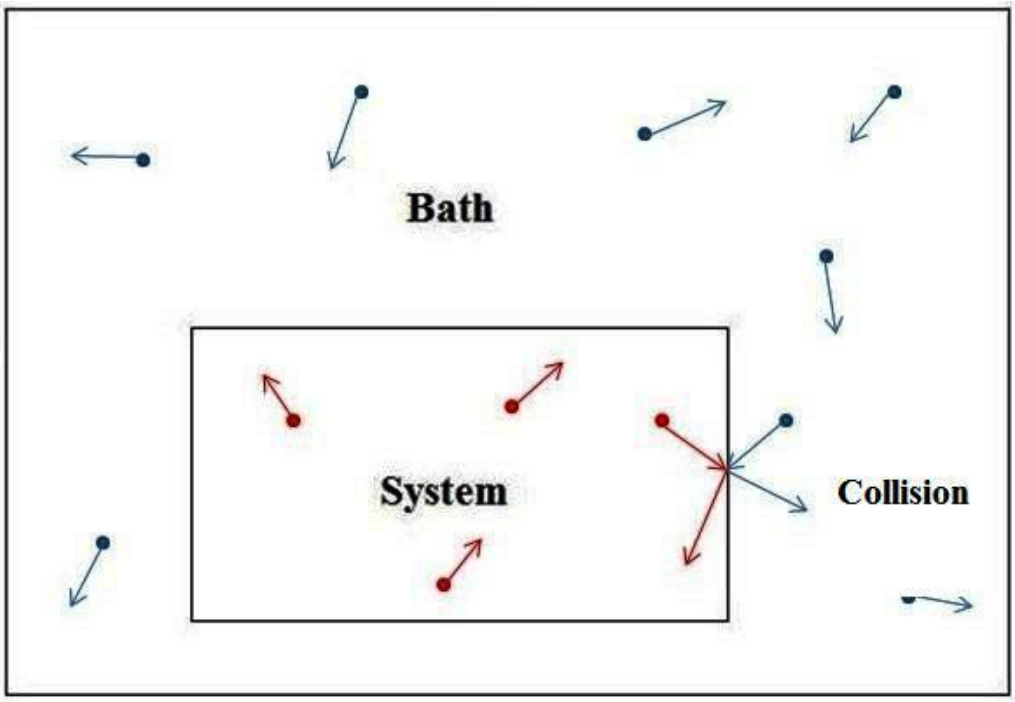

Figure 3.1 Illustration of Constant Temperature Dynamics

3.2 Force Fields

In order to solve equation (3-3), an input, more specifically, a description of the intermolecular interactions is required. It is to use a force field, which is usually derived empirically from experimental data and/or quantum chemical calculations. It makes large scale calculation possible.

Generally speaking, there are three types of force fields. The first type usually has a great coverage of elements in the periodic table. Reasonable results can be obtained from this type of force field; one good example is the force field UFF (Rappe et al., 1992). Another type of force field is capable of providing more precise prediction, but with compromise of the chemical elements coverage. For instance, Cole et al. (2007) introduced a specific force field for studying the hydroxylated silica surfaces, especially its interaction with water molecules. The third type of force field is emphasized on both quality of the prediction and the quantities of force types. These force fields are sophisticatedly parameterized empirically or experimentally. And the COMPASS force field belongs to this type.

The COMPASS (Condensed-phase optimized molecular potentials for atomistic simulation studies) force field was used in our study. It was evolved from the *ab initio* polymer consistent force field (PCFF) which means that most of the parameters of the COMPASS force field are derived from ab initio calculation. The COMPASS force field uses some of the parameters in PCFF, along with some new parameterized molecular classes. According to the accessing and comparison work of Yang et al. (2000), the COMPASS force field is generic force field for condensed phase among the various choices of force

field. Instead of using common LJ 12-6 function for van der Waals (vdw) interaction term, a softer LJ 9-6 function is used in this force field.

The bonded and non-bonded interactions are shown as follows:

$$E_{total} = \sum_b [k_2(b - b_0)^2 + k_3(b - b_0)^3 + k_4(b - b_0)^4] \quad \text{(bond)}$$

$$+\sum_\theta [k_2(\theta - \theta_0)^2 + k_3(\theta - \theta_0)^3 + k_4(\theta - \theta_0)^4] \quad \text{(angle)}$$

$$+\sum_{b,b'} k_{b,b'}(b - b_0)(b' - b_0') \quad \text{(bond-bond)}$$

$$+\sum_{b,\theta} k_{b\theta}(b - b_0)(\theta - \theta_0) \quad \text{(bond-angle)}$$

$$+\sum_{i,j} \frac{q_i q_j}{r_{ij}} \quad \text{(coulombic)}$$

$$+\sum_{i,j} \varepsilon_{i,j}[2(\frac{r_{ij}^0}{r_{ij}})^9 - 3(\frac{r_{ij}^0}{r_{ij}})^6] \quad \text{(vdW)}$$

(3-6)

The COMPASS force field encompasses a large number of atomic force types for oxygen, nitrogen, and carbon atoms, due to the verities of the compounds of these three elements. Properties from MD results of organic solvents using the COMPASS force field have been found to be consistent with experimental data, indicating that it is a superior force field for organic solvents (Sun, 1998). Partial atomic charges of atoms in organic molecules assigned by the COMPASS force field are considered to be fairly reliable (Svard and Rasmuson, 2009).

3.3 Density Functional Theory (DFT)

The COMPASS force field was initially invented for condense phase of organic substances such as polymer and organic liquids. Therefore, partial atomic charges estimated on inorganic materials are not reliable. Density functional theory (DFT)

overcomes this shortcoming. DFT calculations are based on quantum mechanics. More specifically, it is based on a theory that the ground-state properties of a system are functions of the electron density (Hohenberg and Kohn, 1964). The total electronic energy can be written as

$$E(\rho)=E_{KE}(\rho)+ E_C(\rho)+ E_H(\rho)+ E_{XC}(\rho) \quad (3\text{-}7)$$

where $E_{KE}(\rho)$ is the kinetic energy, $E_C(\rho)$ is the electron-nuclear interaction term, $E_H(\rho)$ is the electron-electron Coulombic energy, and $E_{XC}(\rho)$ contains the exchange and correlation contributions. DFT calculations optimize the energy and structure of atoms with respect to the density of the electrons (Leach, 1996).

It is worth pointing out that, approximation for the last term of Eq. 3-7 must be made. This approximation determines the accuracy of the DFT calculations. Local density approximation (LDA) is the simplest way to represent the exchange-correlation functional. LDA assumes that the exchange-correlation energy at any point in space can be given by the electron density of a homogeneous electron gas of the same density. The advantage of LDA is simplicity but it fails for some cases such as hydrogen-bonded systems. Another method is the generalized gradient approximation (GGA). It depends not only on the density but also on the gradient of the density $\Delta\rho(\mathbf{r})$, making GGA closer to the real system because the real system could differ significantly from the homogeneous gas situation (Sousa et al., 2007). The GGA is a good improvement over LDA; in general, GGA tends to give more accurate results for covalent, ionic, metallic and hydrogen bridge bonds (Tao and Perdew, 2005; Patton and Pederson, 1997).

The deficient of GGA is that it is too simple to represent the entire nonlocality of exchange correlation. So Perdew-Wang (PW) correlation functional was developed to address such deficiency (Csonka et al., 1997). Tsuzuki and Luthi (2001) found that the PW91 functional is relatively better method than BLYP and B3LYP functional in calculating interaction energy.

After the DFT calculation, the partial atomic charges of the atoms can be obtained from the wave function analysis. One of the most common wave function analyses is the Mulliken population analysis (Leach, 1996). And it is reported to yield relatively accurate estimation of partial atomic charges for a wide variety of molecular systems (Clark et al., 2004).

3.4 Radial Distribution Function

The structure of liquid can be well characterized by the radial distribution function (or pair correlation function) ($g_{AB}(r)$) as defined by the following equation:

$$g_{AB}(r)=<\rho_B>_{local}/\rho_B(r) \qquad (3\text{-}8)$$

$g_{AB}(r)$ represents the probability of finding atom B within the range r+dr around atom A (Roy, 2008). Wu et al. (2009) used radial distribution function to study the structure of dedecyltrimethylammonium bromide monomolecular layer at the *n*-heptane/water interface, which justified our method using $g_{OH}(r)$ to study the structure of the water monomolecular layer.

3.5 References

Allen, M. P., Tildesley, D. J. (1991) *Computer Simulation of Liquids*, Oxford University Press, New York, NY, 33-39

Andersen, H. C. (1980) Molecular Dynamics Simulations at Constant Pressure and/or Temperature, *Journal of Chemical Physics*, 72, 2384

Ballenegger, V., Arnold, A., Cerda, J. J. (2009) Simulations of non-Neutral Slab Systems with Long-range Electrostatic Interactions in Two-dimensional Periodic Boundary Conditions, *Journal of Chemical Physics*, 131, 9, 094107

Clark, A. E., Sonnenberg, J. L., Hay, P. J., Martin, R. L. (2004) Density and Wave Function Analysis of Actinide Complexes, *Journal of Chemical Physics*, 121, 6, 2563-2570

Cole, D. J., Payne, M. C., Csanyi, G., Spearing, S. M., Ciacchi, L. C. (2007) Development of a Classical Force Field for the Oxidized Si Surface: Application to Hydrophilic Water Bonding, *Journal of the Chemical Physics*, 127, Article # 204704

Csonka, G. I., Nguyen, N. A., Kolossvary, I. (1997) Simple Tests for Density Functional Methods, *Journal of Computational Chemistry*, 18, 12, 1534-1545

Hohenberg, P., Kohn, W. (1964) Inhomogeneous Electron Gas, *Physical Review A*, 136, 864-871

Jorgensen W. L., Tirado-Rives, J. (1996) Monte Carlo vs Molecular Dynamics for Conformational Sampling, *Journal of Physical Chemistry*, 100, 14508-14513

Kohn, W., Sham, L. (1965) Self-Consistent Equations Including Exchange and Correlation Effects, *Physical Review A*, 140, 1133-1138

Leach, A. R., *Molecular Modelling, Principles and Applications*, Addison Wesley Longman Limited, Edinburgh Gate, England

Nielsen, S. O., Srinivas, G., Klein, M. L. (2005) Incorporating a Hydrophobic Solid into a Coarse Grain Liquid Framework: Graphite in an Aqueous Amphiphilic Environment, *Journal of Chemical Physics*, 123, 124907

Parzen, E. (1962) *Stochastic Processes*, Holden-Day, San Francisco, CA, 117-123

Patton, D. C., Pederson, M. R. (1997) Application of the Generalized-Gradient Approximation to Rare-gas Dimers, *Physical Review A*, 56, 2495

Rappe A. K., Casewit, C. J., Colwell, K. S., Goddard, W. A. III, Skiff, W. M. (1992) UFF, a Full Periodic Table Force Field for Molecular Mechanics and Molecular Dynamics Simulations, *Journal of American Chemical Society*, 114, 10024-10035

Roy, P. (2008) Course Notes of Chem 495: Molecular Dynamics and Its Applications, 2008, University of Alberta, AB

Sousa, S. F., Fernandes, P. A., Ramos, M. J. (2007) General Performance of Density Functionals, *Journal of Physical Chemistry A*, 111, 10439-10452

Sun H. (1998) COMPASS: An *ab Initio* Force-Field Optimized for Condensed-Phase Applications—Overview with Details on Alkane and Benzene Compounds, *Journal of Physical Chemistry B*, 102, 7738-7364

Svard M., Rasmuson, A. C. (2009) Force Fields and Point Charges for Crystal Structure Modeling, *Industrial and Engineering Chemistry Research*, 48, 6, 2899-2912

Tao J., Perdew, J. P. (2005) Test of a Nonempirical Density Functional: Short-range Part of the van der Waals Interaction in Rare-gas Dimers, *Journal of Chemical Physics*, 122, Art # 114102

Tsuzuki, S., Luthi, H. P. (2001) Interaction Energies of Van der Waals and Hydrogen Bonded Systems Calculated Using Density Functional Theory: Assessing the PW91 Model, *Journal of Chemical Physics*, 114, 9, 3949-3957

Tuckerman, M. E., Martyna, G. J., (2000) Understanding Modern Molecular Dynamics: Techniques and Applications, *Journal of Physical Chemistry B*, 104, 159-178

Wu, R. Deng, M., Kong, B., Wang, Y., Yang, X. (2009) Molecular Dynamics Simulations of Ammonium Surfactant Monolayers at the Heptane/Water Interface, *Journal of Physical Chemistry B*, 113, 12680-12686

Yang, J., Ren, Y., Tian, A., Sun, H. (20000 COMPASS Force Field for 14 Inorganic Molecules in Liquid Phases, *Journal of Physical Chemistry B*, 104, 4951-4957

Chapter 4

Heat of Immersion

4.1 Introduction

In this chapter, results on the calculations of heats of immersion of various liquids including *n*-heptane, toluene, pyridine and water on model sand and clay surfaces are presented. Heat of immersion signifies the strength of the interaction at the solid/liquid interface. The higher the heat of immersion, the stronger the interaction is between the solvent and surface. The calculated values can be used to determine which solvent has stronger interactions with the model surfaces.

Heat of immersion is usually easy to obtain from experiment; it has become an important parameter in the petroleum reservoir science. In experiment, the solid particles will be immersed in a liquid solvent, and heat of immersion will be obtained from the energy change in this process (Zoungrana et al., 1995). Malandrini et al. (1997) used immersion microcalorimetry to study the interfacial properties of quartz/water and quartz/organic solvents (including *n*-heptane, benzene and pyridine); their results indicated that water has higher heat of immersion on quartz than other organic solvents tested.

Some researchers found that the heat of immersion is highly related to the electrostatic interactions between the surface and the liquid molecules (Medout-Marere et al., 1997; Takei and Chikazawa, 1998). In this chapter, the effect of partial atomic charges of atoms in organic molecules and inorganic surfaces on

the heat of immersion will be discussed. Role of hydrogen bonds, a special type of electrostatic interaction, was also investigated.

4.2 Computational Models and Methods

Heat of immersion can be computed using molecular dynamics simulation as described in the last chapter by the following equations:

$$\Delta E_{imm}=E_{liquid}+E_{surface}-E_{total} \quad (4\text{-}1)$$

$$\Delta H_{imm}=\Delta E_{imm}/A \quad (4\text{-}2)$$

where E_{liquid} and $E_{surface}$ are the internal energies of the liquid layer and mineral surface, while E_{total} is the internal energy of the system containing the liquid layer and the mineral surface. And ΔH_{imm} is the heat of immersion normalized by the interfacial area A. Four types of liquids, two types of sand surfaces and two basal surfaces of kaolinite were employed in the present work. Details about the models used in simulations will be discussed in the following sections.

4.2.1 Model Sand Surfaces

Two silica surfaces were created by cleaving from corresponding silica mineral crystals, alpha quartz and cristobalite, labeled as HWH and HWOH surfaces, respectively. The rationale for the naming of these two surfaces will be given later in section 4.3.1. The cleaving surface for quartz is (0 0 1) while that (1 1 1) for cristobalite. It was shown that the (0 0 1) quartz surface is the most stable surface (Goumans et al., 2007). The reason that we used two different sand surface models is that the concentrations of hydroxyl groups on these two surfaces are

different. Both surfaces were terminated with hydroxyl groups connected to the uncoordinated sites on the cleaving planes. The concentrations of hydroxyl groups on HWH and HWOH surfaces are 9.6×10^{-2} and 4.5×10^{-2} /Å^2, respectively.

The thickness of the HWH surface is 15.6 Å, and that of the HWOH is 21.7 Å. The cross section areas of HWH and HWOH are 188 Å^2 and 200 Å^2, respectively.

4.2.2 Model Clay Surfaces

Our model clay surfaces were cleaved from the kaolinite unit cell from the structure library of Materials Studio version 4.2; the cleaving planes were parallel to the (0 0 1) face in the bulk kaolinite. Octahedral and tetrahedral surfaces were created depending where the structure was cleaved. No substitution or modification of any ions was made to the clay surface model; the total net charge of the clay surface model was set to zero. Four repeating layers of kaolinite were used in such a model and found that it was adequate. Since kaolinite is well known as non-swelling and non-porous, no liquid molecules were introduced in the inter-layer spacing. The clay/liquid interaction was determined only on the octahedral or tetrahedral surface. Cross section areas of octahedral and tetrahedral surfaces are 276 Å^2.

4.2.3 Geometric Optimization of the Model Surfaces

Geometric optimization was done according to the relaxation of the surface energy. The energy convergence tolerance between consecutive steps was set at

1.0×10^{-5} Ha. The mineral model surface layers were both optimized and relaxed by DFT calculations using the CASTEP code available in the Materials Studio software. Generalized gradient approximation and its parameterization of Perdue and Wang (PW91) were used for exchange and correlation. The atoms in the first layer of kaolinite were allowed to adjust their positions while those in the three layers below were fixed during the relaxation. Same optimization was carried out for the aforementioned silica surfaces, but only the hydroxyl groups on the surfaces were allowed to relax.

4.2.4 Liquid Models

One aliphatic liquid (*n*-heptane), two types of aromatic liquids (one is toluene while the other is pyridine), and water were used in this work. The molecular structures and partial atomic charges of these four molecules are shown in Figure 4.1. The partial atomic charges of the atoms were assigned by the COMPASS force field according to the atom type. As mentioned, partial atomic charges of atoms in the COMPASS force field are derived from *ab initio* calculation (Sun, 1998; Sun et al., 1998). The water model incorporated in the COMPASS force field is simple three-point model. Using this model, density of water obtained from *NPT* simulation at 293 K and 0.1 MPa is quite similar with the experimental data (Rigby, 2004).

The Amorphous Cell Tool in Materials Studio was used to construct the liquid layers; the densities used were from experimental data at room temperature. In particular, 0.680 g/ml was used for the density of *n*-heptane (Fang et al., 1991),

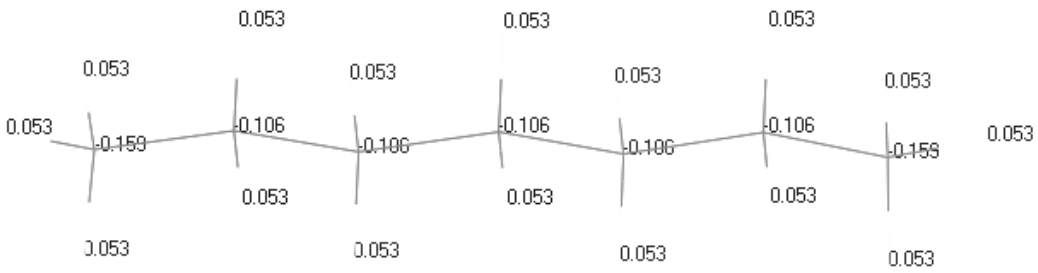

(a) *n*-heptane

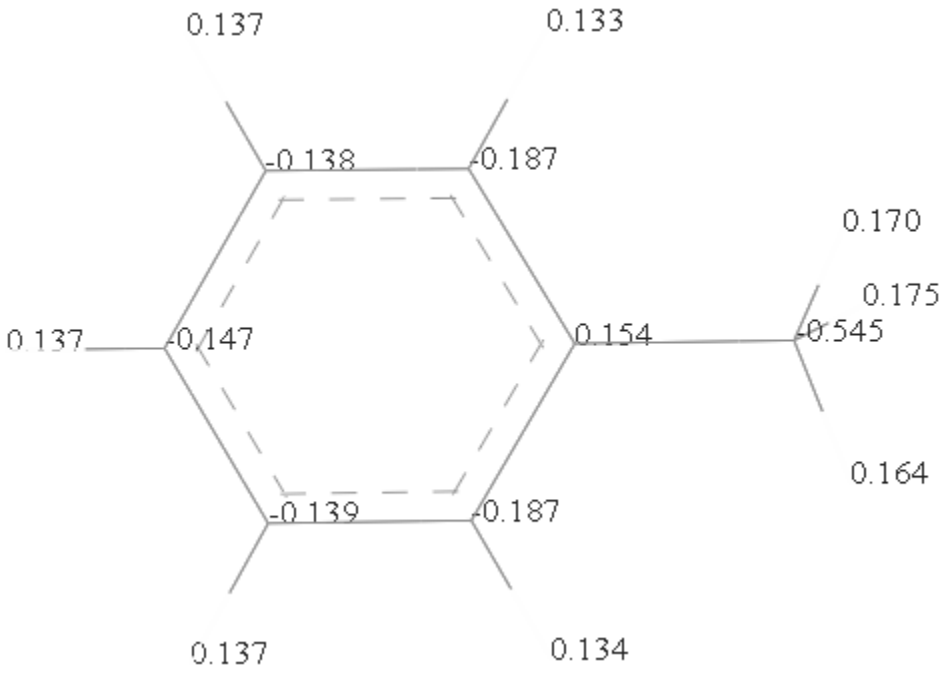

(b) Toluene

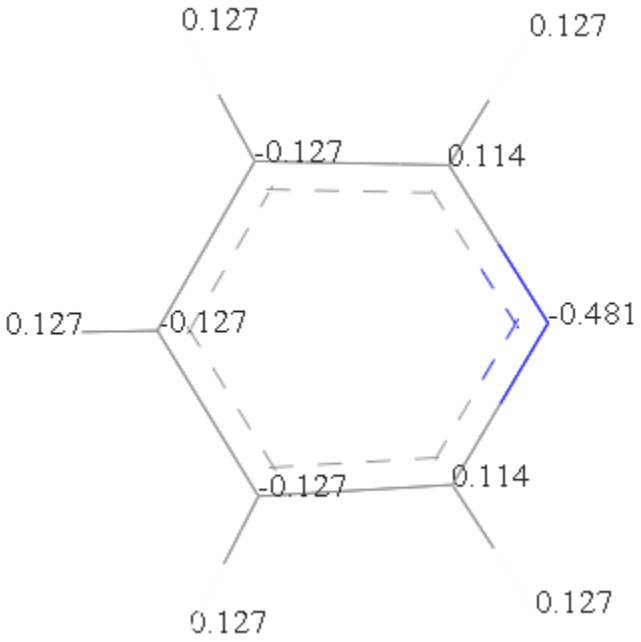

(c) Pyridine

(d) Water

Figure 4.1 Molecular Structures and Partial Atomic Charges of (a) *n*-Heptane (b) Toluene (c) Pyridine (d) Water as Assigned by the COMPASS Force Field

0.862 g/ml was used for the density of toluene (Exarchos et al., 1995; Sporzynski et al, 2005), 0.979 g/ml for pyridine (Nayak et al., 2003), and 0.996 g/ml for water (Incropera et al., 2005), respectively.

The thicknesses of the *n*-heptane, toluene, pyridine and water layers were 16.91 Å, 24.53 Å, 18.55 Å and 21.76 Å, respectively. Such thicknesses are beyond the inter-atomic interaction cutoff distance used for the dispersion forces. These liquid layers were built as thin layers (periodic in the x, y directions, but not in the z direction) and were assembled with the surface layer. The cross-section areas of the liquid layers were set to be the same as the silica or kaolinite model surfaces.

4.2.5 MD Simulation

Since the entire simulation cell (liquid layer + mineral surface) is three dimensional periodic, each cell was assembled with a 90 Å vacuum slab to minimize the forces between the water molecules with the bottom layer of periodic images of the mineral (See Figure 4.2). In literature, 15-25 angstroms of vacuum slabs have been used. However, in our previous work, we have found that vacuum slabs larger than sixty angstroms yielded results that were comparable to experiment. The Cartesian coordinates of all atoms in the mineral surface were fixed in the MD simulation in which organic liquids or water were present in order to save the simulation time.

NVT MD simulations at 298 K and 373 K were carried out by the Discovery code of Materials Studio. A simulation time of 2,000 picosecond (ps)

Figure 4.2 Structure Containing Four Repeating Units of Kaolinite and a Layer of *n*-Heptane with Periodic Images in the Positive y and Positive z Directions

with a time step of 1 femtosecond (fs) was used for each simulation. Based on our previous work, the simulation time is sufficient to equilibrate these systems. The Andersen thermostat was employed in all simulations (Koopman and Lowe, 2006; Kelly et al., 2004).

The interatomic cutoff distance was set at 9.5 Å for vdW potential. It has been shown that the cutoff distance of 2.5σ (the collision diameter σ is the separation distance where the vdW energy is zero) gives rise to a relatively small error (Allen and Tildesley, 1991; Leach, 1996). In the COMPASS force field, the collision diameters for most atom types are below 3.5 Å (for example, σ for carbon atom in aromatic ring is 3.420 Å) (Sun, 1998), so 9.5 Å should be adequate.

In this work, the COMPASS force field was used to assign the atomic force types and partial atomic charges for the liquid molecules and sand model surfaces. However, the partial atomic charges of the kaolinite atoms were assigned by the Mulliken charges as obtained from the DFT calculations (Larin et al., 1998). Long range electrostatic interactions were handled with the Ewald method (Leach, 1996). These MD simulation settings were also used in the latter chapter.

4.3 Results and Discussion

4.3.1 Model Surfaces Relaxation

Optimization was done on both HWH and HWOH surfaces; the surface hydroxyl groups behaved differently on these two model surfaces. Hydrogen bonds were

observed to form between the surface hydroxyl groups on the hydrated quartz (HWH) surface; but this was not the case for the hydrated cristobalite (HWOH) surface as the hydroxyl groups were far apart. This is the reason that cleaved hydrated quartz and critobalite surfaces are labeled as HWH surface (hydrated surface with hydrogen bonds) and HWOH surface (hydrated surface without hydrogen bonds). Here, the hydroxyl groups on the HWOH surface can be seen as 'free' groups (Figure 4.3(b)). Other characteristics of the surfaces are listed in Table 4.1.

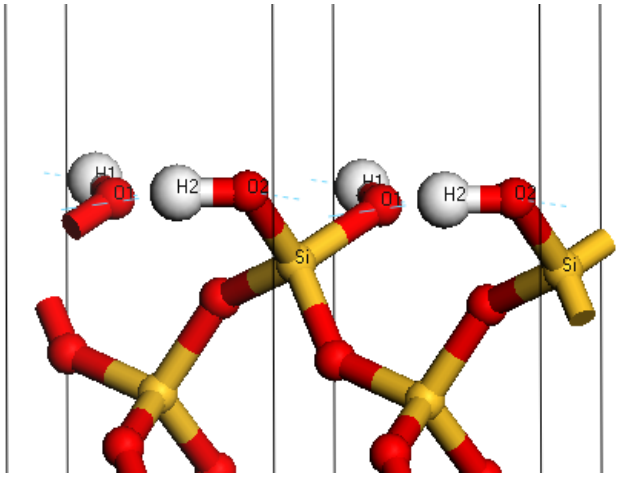

(a)

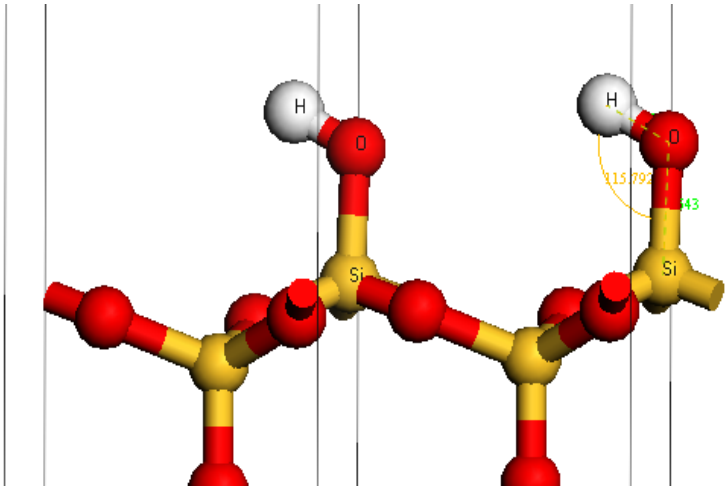

(b)

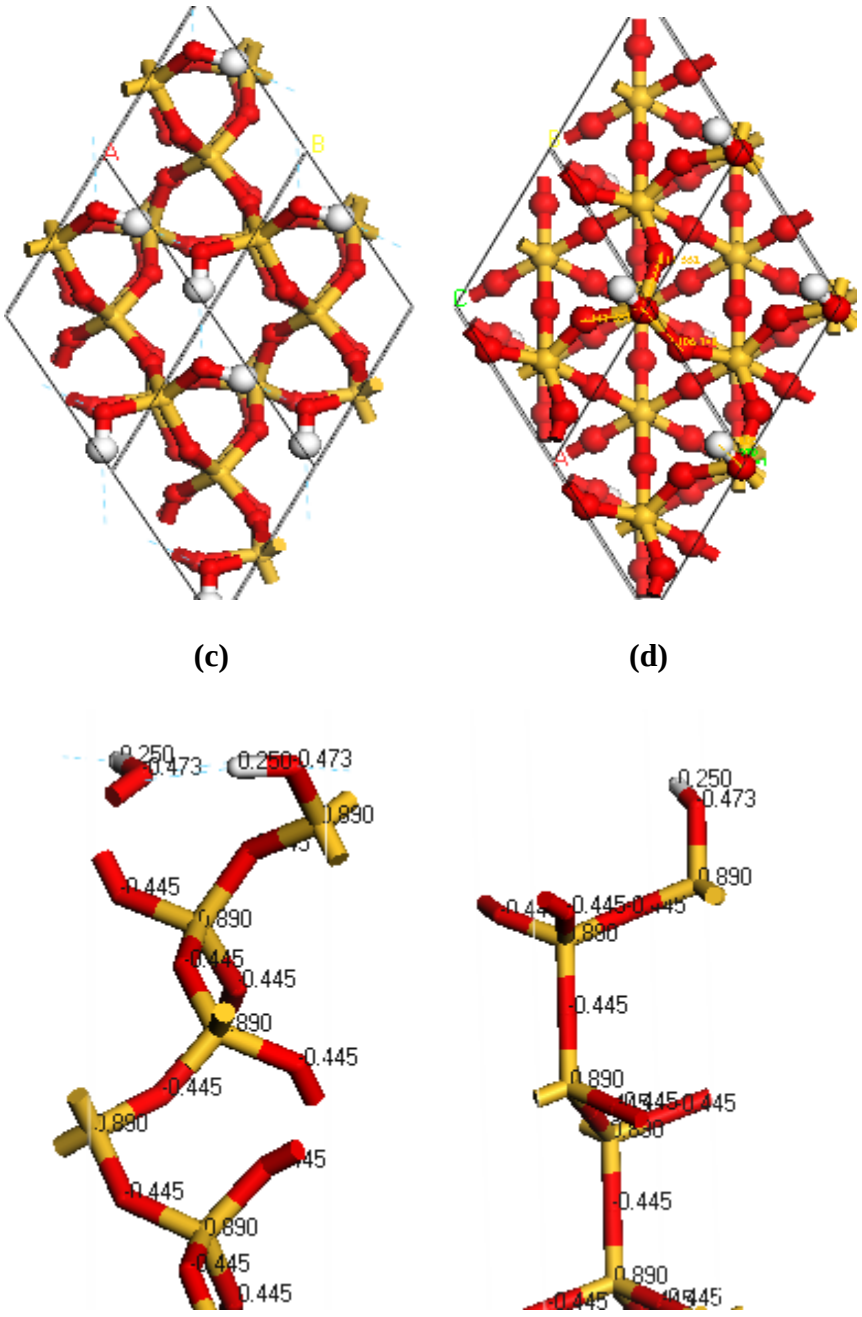

Figure 4.3 Configuration of the atoms in the Relaxed Silica Surfaces (a) HWH Surface (b) HWOH Surface (c) Top View of the HWH Surface (d) Top View of the HWOH Surface and the Partial Atomic Charges of (e) HWH surface and (f) HWOH Surface (White—Hydrogen; Red—Oxygen; Yellow—Silica)

Table 4.1 Geometry Characteristics of Silica Surfaces after Optimization

HWH		HWOH	
Cartesian coordinate in the z direction (Å)		Cartesian coordinate in the z direction (Å)	
H^1	15.534	H	21.673
H^2	15.567	O	21.207
O^1	15.315	Si	19.567
O^2	15.579		
Bond length (Å)		Bond length (Å)	
$r(H^1\text{-}O^1)$	0.985	r(H-O)	0.97
$r(H^2\text{-}O^2)$	0.993	r(Si-O)	1.643
Bond angle (º)		Bond angle (º)	
$Angle(H^1\text{-}O^1\text{-}Si)$	112.5		
$Angle(H^2\text{-}O^2\text{-}Si)$	114.4	Angle(H-O-Si)	115.8

Note that the labeling of the atoms is shown in Figure 4.3(a) & 4.3(b)

The reference of Cartesian coordinate in the z direction is the bottom of the simulation cell.

The coordinates of the atoms in the top kaolinite layer were not fixed during relaxation. After the relaxation, the first layer was elevated slightly. In particular, the space between the first and second layers was expanded by approximately 0.3 Å.

But the most significant change is the orientations of the surface hydroxyl groups. As shown in Figure 4.4(a), there are four types of hydroxyl groups attaching to the aluminum atoms, labeled 1 to 4, respectively. Our results showed that hydroxyl group 2 on the top layer adopted the roughly horizontal position after relaxation. According to the study of Benco et al. (2001a, 2001b), the horizontal position of hydroxyl group 2 on the top layer is the configuration induced by the coupling between the dipoles of hydroxyl group 2 and hydroxyl group 4. However, hydroxyl groups 2 on the lower layers all tend to keep roughly vertical position. This may due to the hydroxyl groups in the second or other inner layers are stabilized by the hydrogen bonds formed between two layers. More details are shown in Table 4.2.

In this work, the hydrogen bonds were determined geometrically among certain donor and accepter atom types defined by the Materials Studio Software. The maximum hydrogen bond donor/accepter distance was set at 2.5 Å, and the minimum donor/accepter angle was 90º.

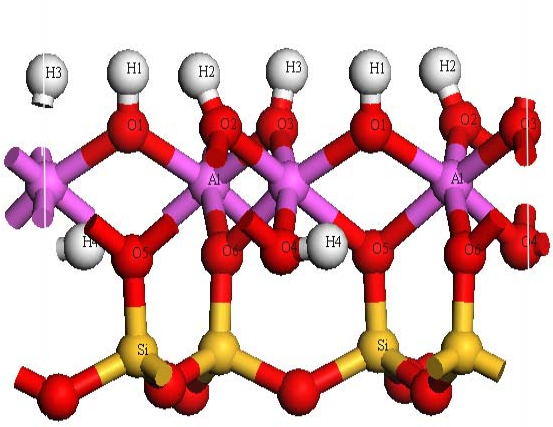
H3
H1
H2
H3
H1
H2
O1
O2
O3
O1
O2
O3
Al
Al
H4
O5
O6
O4
H4
O5
O6
O4
Si
Si

(a)

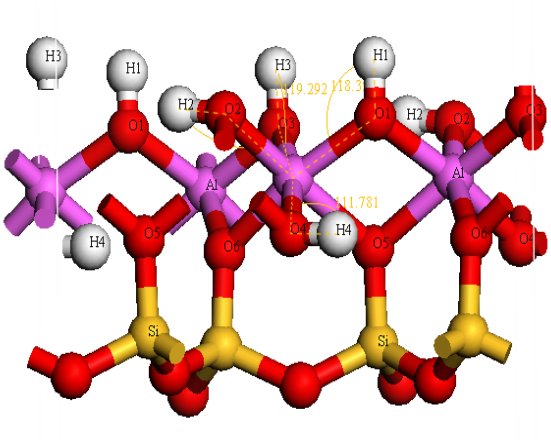
H3
H1
H3
H1
H2
O1
O2
O3
O1
H2
O2
O3
Al
Al
H4
O5
O6
O4
H4
O5
O6
O4
Si
Si

(b)

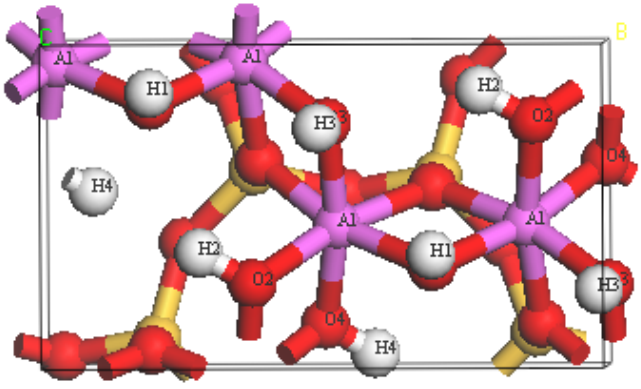
C
B
Al
Al
H1
H2
H3
O2
O4
H4
Al
Al
H2
H1
O2
H3
O4
H4

(c)

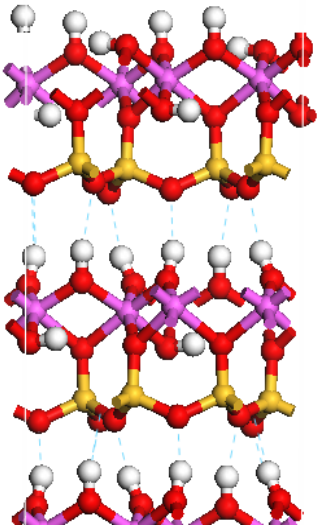

(d)

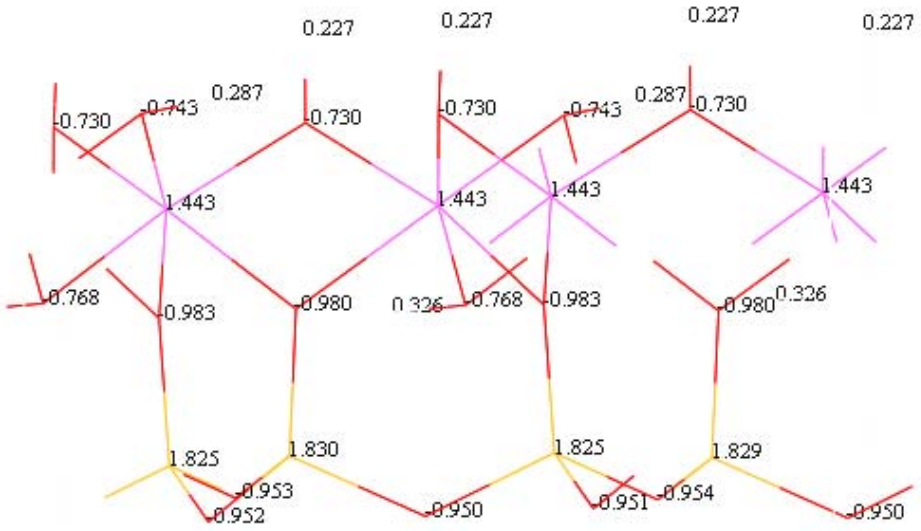

(e)

Figure 4.4 Configuration of Atoms in the First Layer of Kaolinite (a) Before Relaxation (b) Side View After Relaxation and (c) Top view After Relaxation (d)Inter Layer Hydrogen Bonds in Bulk Kaolinite (e) the Partial Atomic Charges of the First Layer (Blue Broken Line—Hydrogen Bonds; Purple—Aluminum)

Table 4.2 Cartesian Coordinates of Atoms in the Top Layer of Kaolinite Before and After Relaxation in the Z Direction

Cartesian coordinates in the z Direction (Å)			
Atom type	Partial atomic charge	Before	After
H^1	0.227	26.70	26.97
H^2	0.287	26.68	26.18
H^3	0.227	26.69	26.97
H^4	0.306	23.84	23.94
O^1	-0.730	25.76	26.00
O^2	-0.743	25.81	26.05
O^3	-0.730	25.76	26.00
O^4	-0.768	23.76	23.99
O^5	-0.980	23.69	23.91
O^6	-0.983	23.69	23.90
Al	1.443	24.84	25.05
Si	1.829	22.08	22.28
Bond angle (°)			
Bond type		Before	After
$Al\text{-}O^1\text{-}H^1$		123.1	118.4
$Al\text{-}O^2\text{-}H^2$		129.0	115.5
$Al\text{-}O^3\text{-}H^3$		127.1	119.3
$Al\text{-}O^4\text{-}H^4$		106.3	111.8

The atoms are labeled as shown in Figure 4.4

4.3.2 Heat of Immersion Results

Heats of immersion calculated from equations (4-1) and (4-2) are shown in table 4.3:

Table 4.3 Calculated Heats of Immersion of *n*-Heptane, Toluene, Pyridine and Water on Sand and Clay Surfaces

n-Heptane		
Surface Type	ΔH_{imm} (mJ/m^2) at 298 K	ΔH_{imm} (mJ/m^2) at 373 K
HWH	104±4	92±3
HWOH	107±5	84±14
Tetrahedral	135±2	107±4
Octahedral	197±6	166±8
Toluene		
Surface Type	ΔH_{imm} (mJ/m^2) at 298 K	ΔH_{imm} (mJ/m^2) at 373 K
HWH	119±8	102±3
HWOH	118±10	98±8
Tetrahedral	163±7	151±3
Octahedral	216±8	208±8
Pyridine		
Surface Type	ΔH_{imm} (mJ/m^2) at 298 K	ΔH_{imm} (mJ/m^2) at 373 K
HWH	119±5	111±5
HWOH	131±8	112±4
Tetrahedral	202±2	179±5
Octahedral	254±10	241±19
Water		
Surface Type	ΔH_{imm} (mJ/m^2) at 298 K	ΔH_{imm} (mJ/m^2) at 373 K
HWH	115±5	N/A
HWOH	215±19	N/A
Tetrahedral	261±11	N/A
Octahedral	295±13	N/A

Here, we also present some selected heat of immersion values from other experimental and computational groups.

Table 4.4 Selected Experimental and Computational Results on the Heats of Immersion

Interface	Experimental (mJ/m^2)	Computational (mJ/m^2)	Our Result (mJ/m^2)
n-Heptane/Quartz	104[a] (300 K)	N/A	104±4 (298 K)
Pyridine/Kaolinite	~400[b] (301 K)	238±4[d] (300 K)	228±10[e] (298 K)
Water/Kaolinite	~480[c] (350 K)	179±3[d] (300 K)	278±13[e] (298 K)

[a] Malandrini et al., 1997

[b] Zougrana et al., 1995

[c] Partyka et al., 1979

[d] Hwang et al., 2001

[e] Average of the heats of immersion on the Octahedral and Tetrahedral surfaces from our MD calculations

Table 4.4 shows that experimental data of the heat of immersion on kaolinite surface are higher than the calculated values of our group and of others. In experiment, all types of surfaces of clay particles including both basal surfaces and the edges of the repeating layers are wetted. Since water and organic solvents shows much higher affinity for the edge surfaces (Croteau et al., 2009). Compared with the data from calculation values from us and other group, heat of immersion of pyridine on kaolinite is comparable with others (Zougrana et al., 1995). But for water on kaolinite, our data is higher. It could be caused by the short simulation

time and thinner kaolinite surface used in their MD simulation. Hwang et al. (2001) used three repeating layers and 200 ps in their simulations.

4.3.3 Electrostatic Interactions

The electrostatic interaction was found to be a major factor that determines heat of immersion (Medout-Marere et al., 1997; Takei and Chikazawa, 1998). Compared with silica surfaces, organic solvents and water show stronger affinity for clay surfaces. The partial atomic charges of atoms in clay surfaces are significantly higher than those of the silica surfaces (Figures 4.3 and 4.4); this leads to stronger electrostatic interactions between the model liquids and surfaces. The existence of Aluminum (Al) atoms in the kaolinite repeating layer may also make their contributions as Li and Choi (2007) found that Al atoms exhibit strong interactions with normal alkanes.

The partial atomic charges of atoms in the liquid molecules are also a major factor that affects the heat of immersion value. Among the four solvents, *n*-heptane shows the weakest interaction with mineral surfaces while water is the strongest. From Figure 4.1, for *n*-heptane, the partial atomic charges of hydrogen and oxygen are lowest among four solvents, so its heat of immersion is the lowest. The highly negatively charged nitrogen atom in the pyridine molecule increases the permanent dipole moment of the molecule, heat of immersion of the pyridine is the higher than the other aromatic solvent, toluene. For water, the partial atomic charges of both oxygen and hydrogen atoms are largest, significantly increasing the electrostatic interaction between water and model surfaces. Thus water

exhibited the highest heat of immersion values, the above results suggest that there is a high possibility that a water layer could exist on the mineral model surfaces encountered in oil sands.

4.3.4 Hydrogen Bonds—A Specific Type of Electrostatic Interaction

Besides the chemical composition and partial atomic charges of the substrate and solvent, the existence of surface hydroxyl groups could also affect the heat of immersion. The mechanism is that these groups could form interfacial hydrogen bonds.

The hydrogen bond refers to the attractive electrostatic interaction of a hydrogen atom with an electronegative atom such as nitrogen, oxygen (iupac.org, 1997). It is interesting to point out that the COMPASS force field does not use a separate intermolecular interaction term to describe hydrogen bond; rather, it is included in the calculation of the electrostatic interaction. However, the software we used (Materials Studio) can be used to visualize the hydrogen bonds so long as the hydrogen/acceptor distance is below 2.5 Å and the hydrogen/acceptor angle is above 90º. Here, the acceptors can be sulfur, oxygen, nitrogen atoms.

There are two types of hydrogen bonds observed in these calculations. The first type is the one formed between certain types of atom(s) in the liquid molecules and the surface hydroxyl groups denoted as interfacial hydrogen bonds. Not all surface hydroxyl groups can form interfacial hydrogen bonds; the HWH surface (Figure 4.5(a)), despite having a high number of surface hydroxyl groups, it can not form hydrogen bonds with the solvent molecules (no free hydroxyl

groups). Only the free hydroxyl groups can form interfacial hydrogen bonds and increase the heat of immersion. They exist on the HWOH and octahedral surfaces (Figure 4.5(b) and (c)). For instance, heats of immersion of toluene on the HWH and HWOH surfaces are quite comparable, which is also observed for *n*-heptane (no interfacial hydrogen bonds on either surface). However, heat of immersion of pyridine or water on the HWOH surface is higher than that on the HWH surface (no interfacial hydrogen bonds on HWH surface). These interfacial hydrogen bonds were also found from the snapshots of water simulations (Figure 4.5(d)).

The second type is water/water hydrogen bonds, which do not exist in the other three solvents. Unlike pyridine, water molecules contain both hydrogen bond donors and acceptors. The hydrogen bonds between water molecules in the bulk play an important role in determining the properties of this liquid (Teixeira et al., 2006). In fact, water molecules form a network of hydrogen bonds in the liquid state (Devereux and Popelier, 2007). In the simulations of water layer on the octahedral surface, the number of interfacial hydrogen bonds is 4±2, while that of water/water hydrogen bonds is about 200±20 in the water layer.

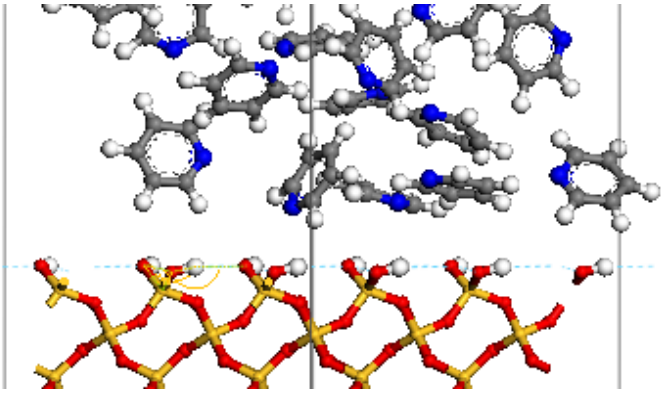

(a)

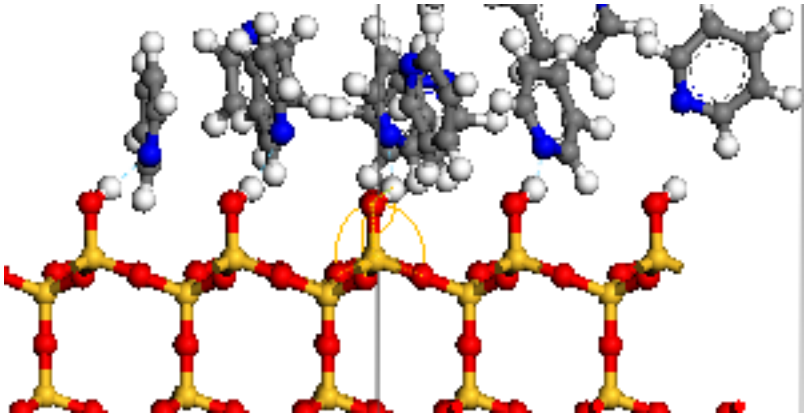

(b)

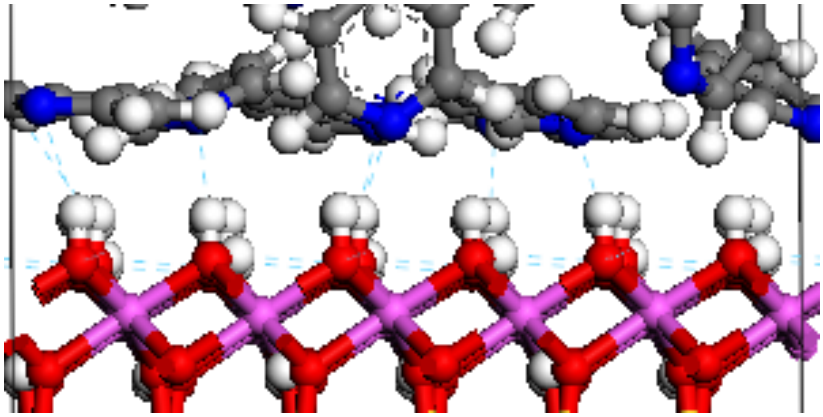

(c)

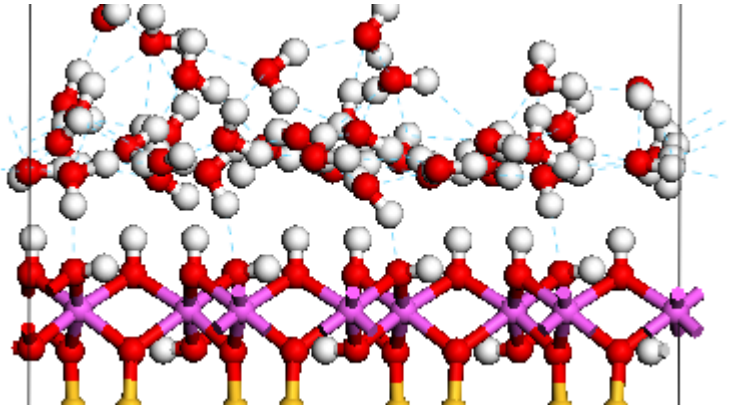

(d)

Figure 4.5 Typical Snapshots from Simulations of (a) Pyridine on HWH Surface (No Interfacial Hydrogen Bonds) (b) Pyridine on HWOH surface (c) Pyridine on the Octahedral surface (d) Water on Octahedral surface (Interfacial Hydrogen Bonds and Water/Water Hydrogen Bonds)

4.4 Summary

The calculations showed that *n*-heptane has the lowest affinity for the model sand and clay surfaces; while water is the highest among the four solvents tested. This suggests that water layers could exist in the raw oil sands. Our data showed that heat of immersion was related to the electrostatic interactions including hydrogen bonds. Meanwhile, in the simulation of water case, the unique network of hydrogen bonds was observed. In order to study the effects of this network on the affinity of water for model clay surfaces, more simulation results of water on the kaolinite basal surfaces will be reported in the next chapter.

4.5 References

Allen, M. P., Tildesley, D. J. (1991) *Computer Simulation of Liquids*, Oxford University Press, New York, NY, 28-29

Benco, L., Hafner, D. T., Lischka, H. (2001a) Upper Limit of the O-H•O Hydrogen Bond. *Ab Initio* Study of the Kaolinite Structure**,** *Journal of Physical Chemistry B*, 105, 10812-10817

Benco, L., Hafner, D.T., J., Lischka, H. (2001b) Orientation of OH groups in kaolinite and dickite: Ab initio molecular dynamics study, *American Mineralogist*, 86, 1057-1086

Croteau, T., Bertram A. K., Patey, G. N. (2009) Simulation of Water Adsorption on Kaolinite under Atmospheric Conditions, *Journal of Physical Chemistry A*, 113, 7826-7833

Devereux, M., Popelier, P. L. A. (2007) The Effects of Hydrogen-Bonding Environment on Polarization and Electronic Properties of Water Molecules, *Journal of Physical Chemistry A*, 111, 1536-1544

Exarchos, N. C., Tasioula-Margar, M., Demetropoulos, I. N. (1995) Viscosties and Densities of Dilute Solutions of Glycerol Trioleate+Octane+p-Xylene+Toluene, and Chloroform, *Journal of Chemical and Engineering Data*, 40, 567-571

Fang S., Zhao C., He C. (2008) Densities and Viscosities of Binary Mixtures of Tri-*n*-butyl Phosphate + Cyclohexane, + *n*-Heptane at T=(288.15K, 293.15, 298.15, 303.15, and 308.15) K, *Journal of Chemical and Engineering Data*, 53, 2244-2246

Goumans, T. P. M., Wander, A., Brown, W. A., Catlow, C. R. A. (2007) Structure and Stability of the (0 0 1) α-Quartz surface, *Physical Chemistry Chemical Physics*, 9, 2146-2152

Hwang, S., Blanco, M., Demiralp, E., Cagin, T., Goddard, W. A. (2001) The MS-Q Force Field for Clay Minerals: Application to Oil Production, *Journal of Physical Chemistry B*, 105, 4122-4127

Incropera, F. P., Dewitt, D. P. (2007) *Introduction to Heat Transfer*, 5th Edition, John Wiley & Sons, Hoboken, NJ

IUPAC website, Hydrogen bond, Compendium of Chemical Terminology (Internet edition)

http://old.iupac.org/publications/compendium/H.html

Kelly, E., Seth, M., Ziegler, T. (2004) Calculation of Free Energy Profiles for Elementary Bimolecular Reactions by ab Initio Molecular Dynamics: Sampling Methods and Thermostat Considerations, *Journal of Physical Chemistry A*, 108, 12, 2167-2180

Koopman, E. A., Lowe, C. P. (2006) Advantages of a Lowe-Andersen Thermostat in Molecular Dynamics Simulations, *Journal of Chemical Physics*, 124, 204103

Larin, A. V., Leherte, L., Vercauteren, D. P. (1998) Approximation of the Mulliken-Type Charges for the Oxygen Atoms of All-Siliceous Zeolites, *Chemical Physics Letters*, 287, 169-177

Leach, A. R., *Molecular Modelling, Principles and Applications*, Addison Wesley Longman Limited, Edinburgh Gate, England

Li C., Choi P. (2007) Molecular Dynamics Study of the Adsorption Behavior of Normal Alkanes on a Relaxed α-Al_2O_3 (0001) Surface, *Journal of Physical Chemistry C*, 111, 1747-1753

Malandrini, H., Sarraf, R., Faucompre, B., Partyka, S., Douillard, J. M. (1997) Characterization of Quartz Particle Surfaces by Immersion Calorimetry, *Langmuir*, 13, 1337-1341

Medout-Marere, V., Belarbi, H., Thomas, P., Morato, F., Giuntini, J. C., Douillard, J. M. (1997) Thermodynamic Analysis of the Immersion of a Swelling Clay, *Journal of Colloid and Interface Science*, 202, 139-148

Nayak, J. N., Aralaguppi, M. I., Toti, U. S., Aminabhavi, T. M. (2003) Density, Viscosity, Refractive Index, and Speed of Sound in the Binary Mixtures of Tri-n-butylamine+Triethylamine, +Tetrahydrofuran, +Tetradecane,

+Tetrachloroethylene, +Pyridine, or +Trichloroethylene at (298.15, 303.15, and 308.15) K, *Journal of Chemical and Engineering Data*, 48, 1483-1488

Partyka, S., Rouquerol, F., Reuquerol, J. (1979) Calorimetric Determination of Surface Areas: Possibilities of a Modified Harkins and Jura Procedure, *Journal of Colloid and Interface Science*, 21-31

Rigby, D. (2004) Fluid Density Predictions Using the COMPASS Force Field, *Fluid Phase Equilibria*, 217, 77-87

Sporzynski, A., Hofman, T., Miskiewiez, A., Strutynska, A., Synoradzki, L. (2005) Vapor-Liquid Equilibrium and Density of the Binary System 1-Phenylethylamine+Toluene, *Journal of Chemical and Engineering Data,* 50, 33-35

Sun H. (1998) COMPASS: An *ab Initio* Force-Field Optimized for Condensed-Phase Applications—Overview with Details on Alkane and Benzene Compounds, *Journal of Physical Chemistry B*, 102, 7738-7364

Sun, H., Ren, P., Fried, J. R. (1998) COMPASS Force Field: Parameterization and Validation for Phosphazenes, *Computational and Theoretical Polymer Science*, 8, 1-2, 229-246

Takei, T. and Chikazawa M. (1998) Origin of Differences in Heats of Immersion of Silicas in Water, *Journal of Colloid and Interface Science*, 208, 570-574

Teixeira, J., Luzar, A., Longeville, S. (2006) Dynamics of Hydrogen Bonds: How to Probe Their Role in the Unusual Properties of Liquid Water, *Journal of Physics: Condensed Matter*, 18, 2353-2362

Zoungrana, T., Berrada, A., Douillard, J. M., Partyka, S. (1995) Competitive Interactions between Water and Organic Solvents onto Mineral Solid Surfaces Studied by Calorimetry, *Langmuir*, 11, 1760-1767

Chapter 5

Behaviors of Water Molecules Adjacent to the Octahedral Surface

5.1 Introduction

As shown in the last chapter, water exhibited the highest heat of immersion value compared to those of *n*-heptane and two aromatic solvents, for both sand and clay surfaces except HWH model surface, suggesting that a water layer could exist on such surfaces. In order to validate the use of the concept of heat of immersion to rank the affinity of various liquids for the mineral surfaces, further MD simulations of a water layer in the absence and presence of the chosen organic solvents were carried out on the octahedral surface of kaolinite. The octahedral surface was chosen as all liquids studied in Chapter 4 exhibited the strongest affinity for such a surface. MD simulations done by Wang et al. (2009) indicated that density of water reduced by 9-15% within 10 Å from the talc surface. Scolowski and Delville (1993) simulated the adsorption of vapor phase water on a montmorillonite surface by using grand canonical Monte Carlo (GCMC) method and found that water molecules in the wetting film near the interface (approximately 10 Å) shows significant difference in density and configuration from the bulk. These results indicate that water adjacent to an interface could have different behaviors.

The second part of this chapter will show the results on systems containing one molecular layer of water on which a molecular layer of organic solvent was presented. These calculations illustrate which liquid could be preferably adsorbed

on the octahedral surface. Similar research has been carried out during the last few decades. MD simulation of 80 cyclohexane molecules and 320 water molecules in the presence of a kaolinite octahedral and tetrahedral surface done by Van Duin and Larter (2001) indicated that a fully water-wet kaolinite is thermodynamically preferable. In the same work, MD simulation of a system containing one benzocarbazole isomer and a water layer containing 333 water molecules adjacent to both octahedral and tetrahedral surfaces of kaolinite surfaces indicated that the benzocarbazole isomer is more favorable to adsorb on rather than desorbing from the surfaces.

5.2 Simulations of Water Layer on Kaolinite Surfaces

5.2.1 Calculation Methods and Models

In this section, we present MD results on one molecular layer of water on the octahedral and tetrahedral surfaces. The relaxed model octahedral and tetrahedral surfaces of kaolinite used in Chapter 4 were used here as well. Two mono-layer water models were built in which different numbers of water molecules were used to cover the clay surfaces with the same dimension. The first one is a mono-layer with 40 waters; this number was chosen in order to construct a planar monomolecular water layer having a density comparable to that of bulk water at room temperature. The other model contained only 20 water molecules with them distributing evenly over the surfaces. Obviously, the density of water in this layer is lower than that of liquid water at room temperature. Both water layer were assembled on top of the model clay surfaces. MD simulations were carried out

using the same force field, simulation temperature and simulation time as those used in the heat of immersion calculations.

5.2.2 Structures of Water on the Octahedral and Tetrahedral Surfaces

A typical snapshot of the configuration of 20 water molecules on the octahedral surface is shown in Figure 5.1. Atoms in the clay shown in Figure 5.1(b) are labeled as light yellow regardless of the atomic species for view convenience. It is clear from the snapshot of the simulation, water molecules tend to form a more compact layer and move closer to each other. Water/water hydrogen bonds play an important role in forming this configuration. Before the simulation, the number of water/water hydrogen bonds was 2/100 $Å^2$; no interfacial hydrogen bond was observed. After 2,000 ps of MD annealing, the number of water/water hydrogen bonds was 10±4/100 $Å^2$; the number of water/surface hydrogen bonds was 2±1/100$Å^2$. The partial atomic charges of oxygen and hydrogen atoms in water molecules are -0.820 and 0.410, respectively, compared with the charges (-0.743 and 0.227) of those atoms in the kaolinite surface hydroxyl groups, causing the electrostatic interaction of water themselves to be stronger than the water-clay surface interaction (See Figure 4.1(d) and 4.4(d)). This leads to water molecules to form more water/water hydrogen bonds than the interfacial hydrogen bonds. From this calculation, the influence of water/water hydrogen bonds on the behavior of water layer adjacent to the model clay surface is obvious. Water molecules tend to form more hydrogen bonds to minimize the liquid energy.

MD simulations of the system containing 40 water molecules on both clay model surfaces were carried out. Comparing the respective initial structures (Figures 5.2 and 5.3), water molecules on the octahedral surface still cover significant amount of the surface after 2,000 ps of MD annealing (Figure 5.4) while in the case of the tetrahedral surface, water molecules tend to cluster more (Figure 5.5). The above results simply suggested that both kaolinite surfaces are hydrophilic with the tetrahedral surface less hydrophilic.

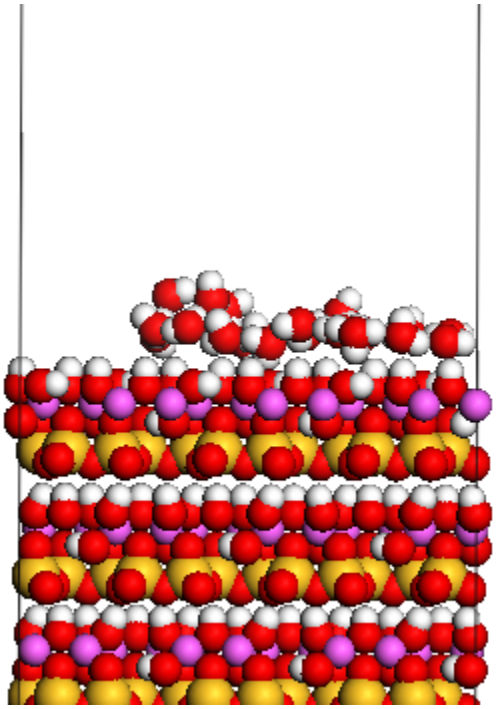

(a)

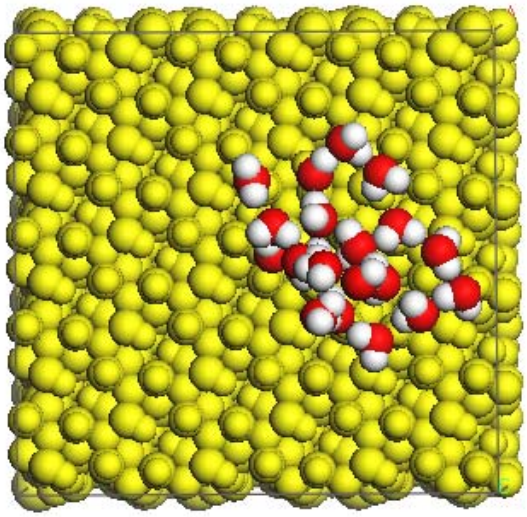

(b)

Figure 5.1 A Typical Snapshot of 20 Water Molecules on the Octahedral Surface upon 2,000 ps of MD Annealing (a) Side View (b) Top View

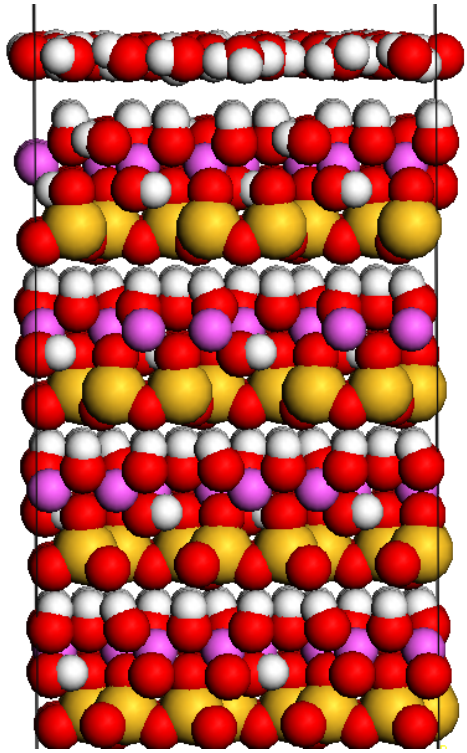

(a)

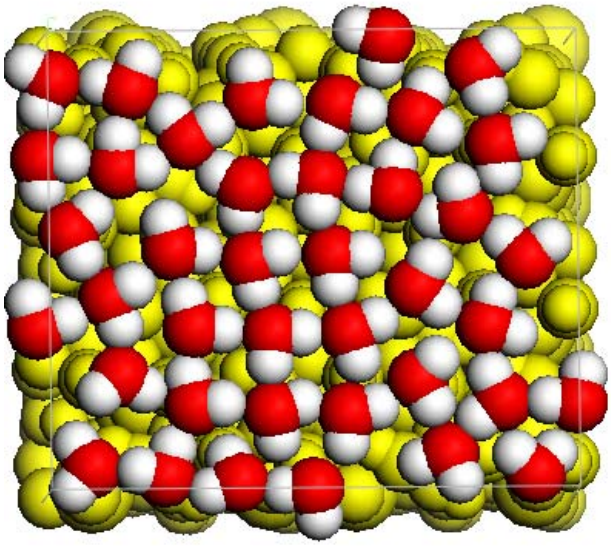

(b)

Figure 5.2 Initial Structure of a Water Monomolecular Layer (40 Water Molecules) on the Octahedral Surface (a) Side View (b) Top View

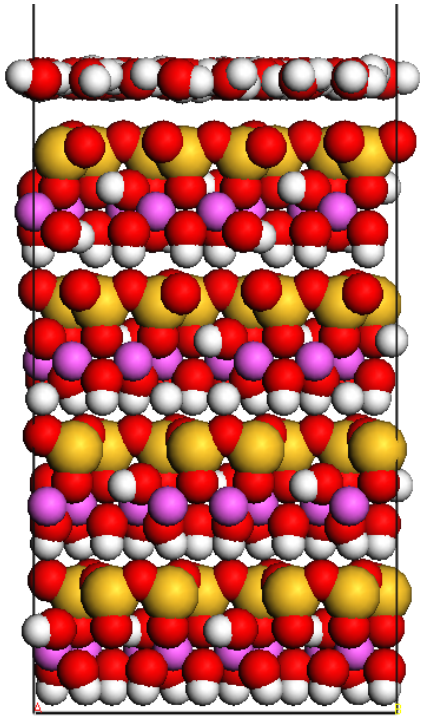

(a)

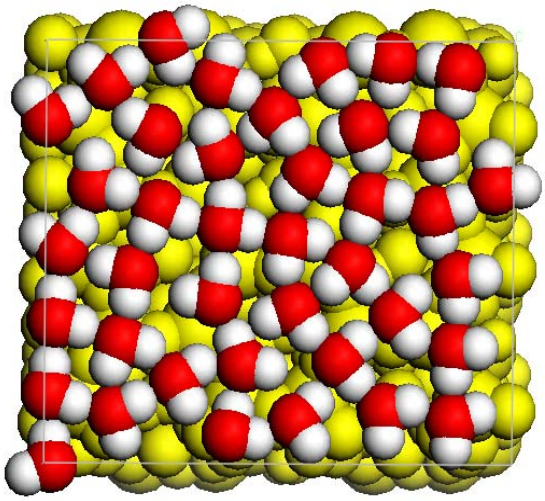

(b)

Figure 5.3 Initial Structure of a Water Monomolecular Layer (40 Water Molecules) on the Tetrahedral Surface (a) Side View (b) Top View

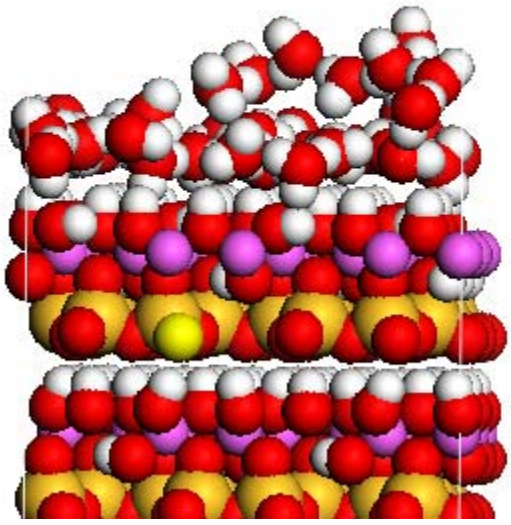

(a)

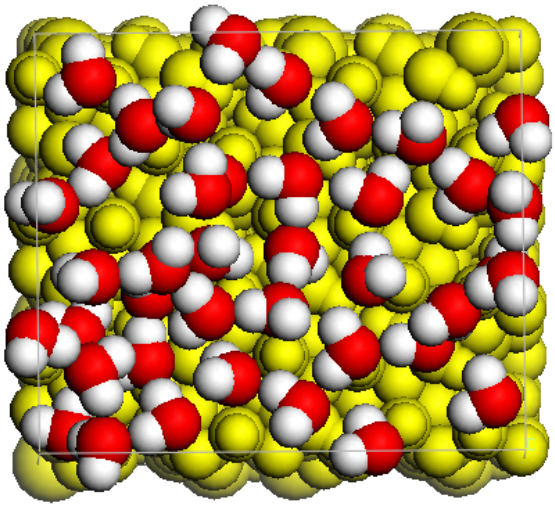

(b)

Figure 5.4 Structure of a Water Monomolecular Layer (40 Water Molecules) on the Octahedral Surfaces upon 2,000 ps of MD Annealing (a) Side View (b) Top View

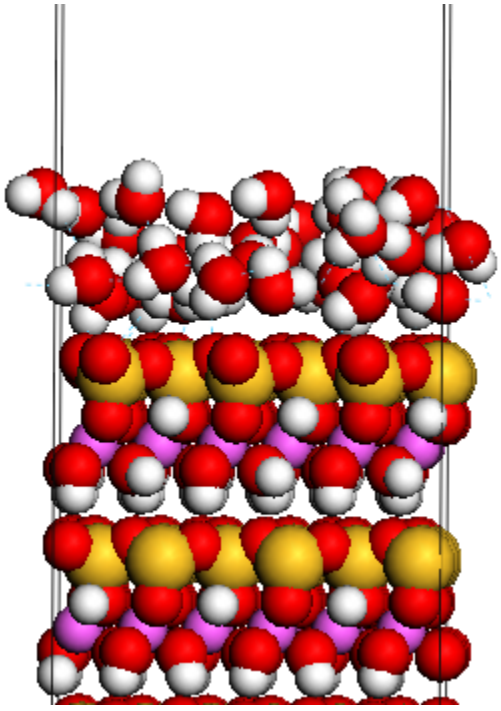

(a)

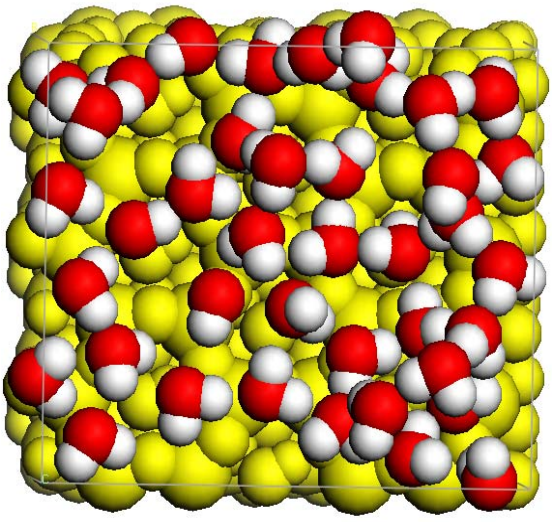

(b)

Figure 5.5 Structure of a Water Monomolecular Layer (40 Water Molecules) on the Tetrahedral Surfaces upon 2,000 ps MD Annealing (a) Side View (b) Top View

In Materials Studio 4.2, the concentration profile of water is determined by taking the Z coordinates of the oxygen atoms as input and "relative concentration" is generated. The so-called "relative concentration" at one given Z coordinate is obtained by dividing the number of the oxygen atoms in the X-Y plane at this Z coordinate by the average number of oxygen atoms per unit thickness of the simulation cell in the Z direction. The water concentration profile corresponding to the system shown in Figure 5.1 indicates that initially water molecules were evenly distributed over the surface with an average distance of 4.5 Å (the broken curve in Figure 5.6). After 2,000 ps, the concentration profile curve evolves to the solid curve shown in Figure 5.6. It is asymmetrical and its major peak is about one angstrom closer to the surface, indicating that water molecules adsorbed strongly on the surface; meanwhile, a few molecules were located in the second molecular layer leading to two peaks on the concentration profile. As mentioned in Chapter 4, this strong affinity is due to the strong electrostatic interaction, not to the interfacial hydrogen bonds. The concentration profile essentially means that water molecules formed more or less a mono-molecular layer on the octahedral surface.

The solid curve in Figure 5.7 shows the water concentration profile of the system shown in Figure 5.4. It resembles the solid curve shown in Figure 5.6. Also, the primary peak indicates that majority of the water molecules were adsorbed on the surface, forming a monolayer which covering the entire octahedral surface. Monolayer of water molecules adsorbed on the octahedral

surface was also observed by other researchers using GCMC (Croteau et al., 2009).

The simulation of water monolayer on the kaolinite tetrahedral surface was also conducted. As can be seen from the dashed curve in Figure 5.7, there are two peaks on the curve indicating that waters on the tetrahedral surface formed a looser configuration—two molecular layers, rather than one as seen in the octahedral surface case. However, the location of the peak on the left indicates that the distance of first layer of water molecules from the tetrahedral surface is comparable to that of the octahedral surface. The difference between the octahedral and tetrahedral curves signifies that the octahedral surface is more hydrophilic than the tetrahedral surface. This simulation result is consistent with our calculated heat of immersion values (Chapter 4). Delville (1995) used GCMC simulation to study structures of adsorbed water films on three clay model surfaces including kaolinite, potassium-mica and sodium-montmorillonite. His results demonstrated that the tetrahedral surface exhibits the lowest affinity for the water molecules. Since the density of the wetting film on the kaolinite tetrahedral surface was the lowest and some water molecules propagated away from the surface.

Water seems to be stable by itself on the octahedral and tetrahedral surfaces. In the following section, calculations on systems containing one water layer and one organic solvent layer on the octahedral surface will be discussed.

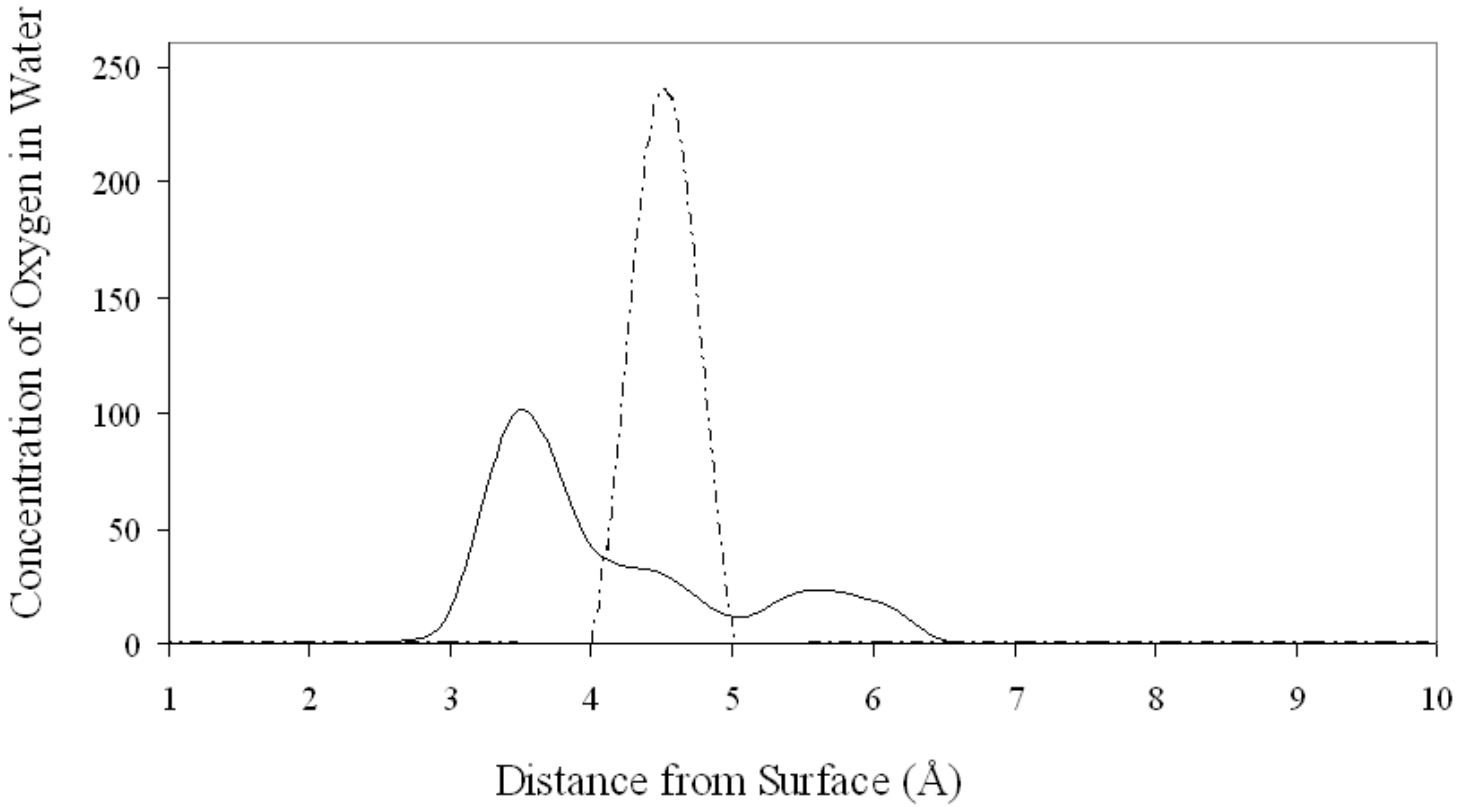

Figure 5.6 The Concentration Profile of Oxygen Atoms in the Layer with 20 Water Molecules during the Simulation Long Dash Dot--Initial Concentration Profile of Oxygen Atoms in Water Layer; Solid--Concentration Profile after the Simulation (2,000 ps)

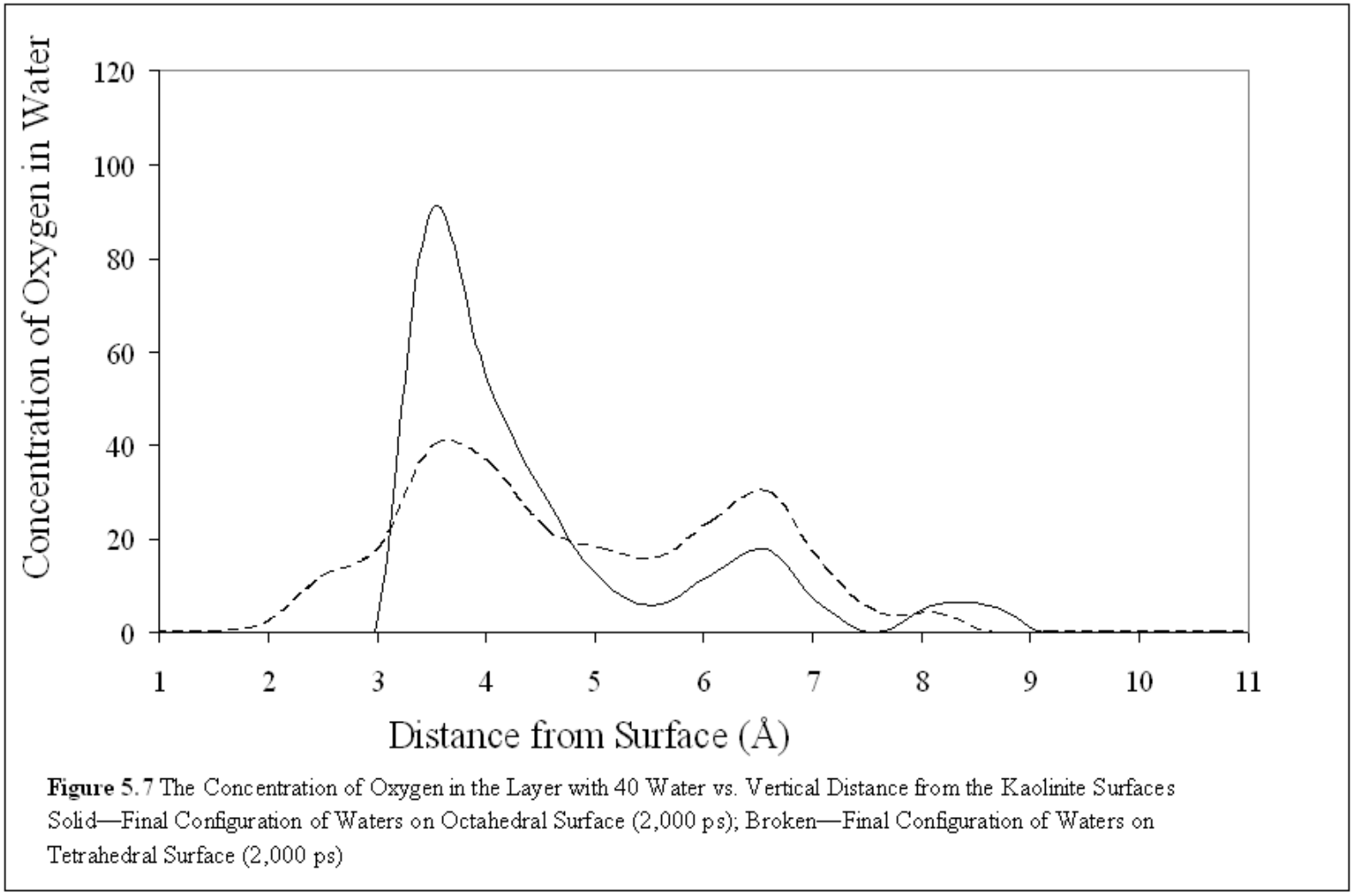

Figure 5.7 The Concentration of Oxygen in the Layer with 40 Water vs. Vertical Distance from the Kaolinite Surfaces Solid—Final Configuration of Waters on Octahedral Surface (2,000 ps); Broken—Final Configuration of Waters on Tetrahedral Surface (2,000 ps)

5.3 Wettability of Water in the Presence of Organic Molecules

5.3.1 Wetting of Water Monomolecular Layer in the Presence of Organic Molecules

MD simulations of surface above which there were two layers of liquids (one molecular layer of water plus that of an organic solvent) were conducted on the octahedral surface. The octahedral surface was chosen as it exhibited the strongest affinity for the four liquids studied in Chapter 4. The water layers with two thicknesses were used. In the first case, the water layer was one molecular layer thick (40 water molecules). The second one was constructed with 100 water molecules; the thickness was 10.87 Å which is about half of the thickness of the water layer used in the heat of immersion calculation (21.76 Å). The results of this multi-molecular water layer will be presented in section 5.3.3. The organic solvent layers were one molecular layer thick consisted of eight solvent molecules of (*n*-heptane, toluene or pyridine). The water layer was adjacent to the octahedral surface while the organic solvent layer was assembled above the water layer. MD simulation settings were the same as those used in the heat of immersion calculations. Figures 5.8, 5.9 and 5.10 show that after about 2,000 ps of MD annealing, toluene and pyridine adsorbed on the surface indicating that both aromatic solvents exhibit stronger affinity for the octahedral surface than water.

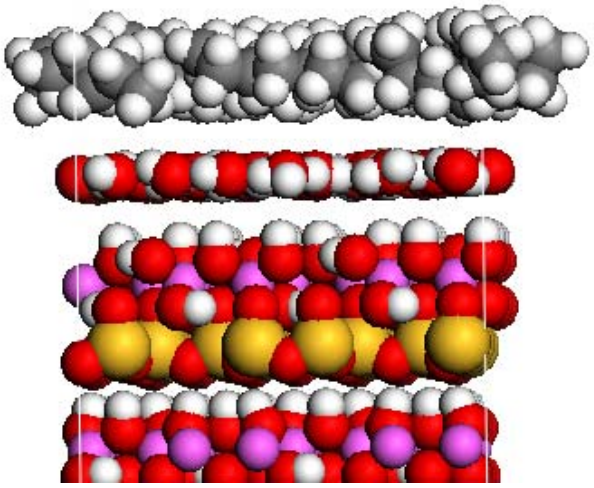

(a)

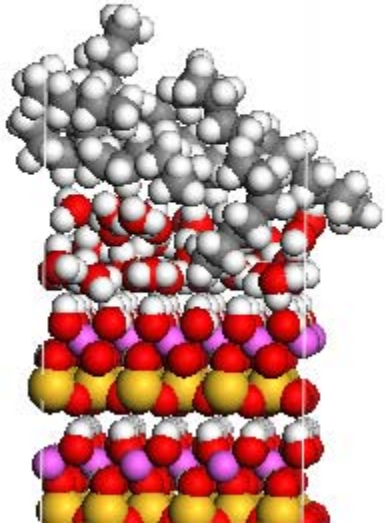

(b)

Figure 5.8 8 *n*-Heptane Molecules and 40 Water Molecules on the Octahedral Surface (a) Before and (b) After 2,000 ps of MD Annealing

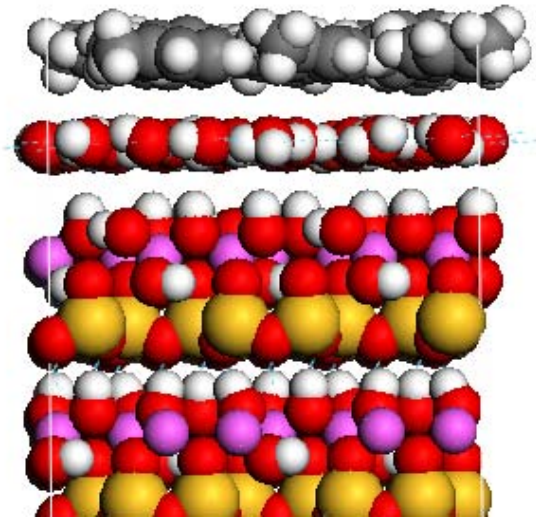

(a)

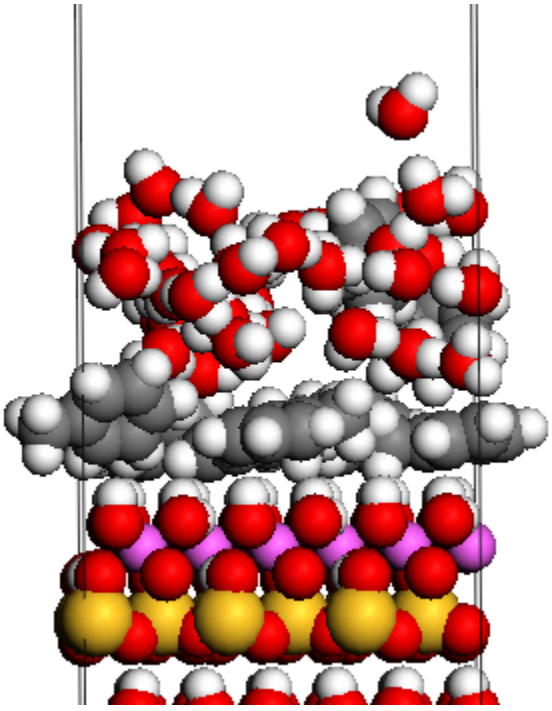

(b)

Figure 5.9 8 Toluene Molecules and 40 Water Molecules on the Octahedral Surface (a) Before and (b) After 2,000 ps of MD Annealing

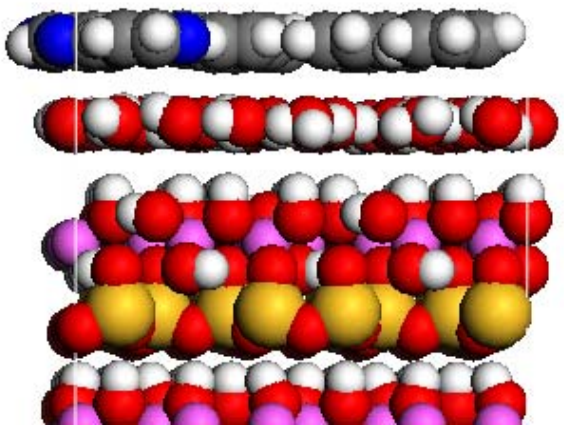

(a)

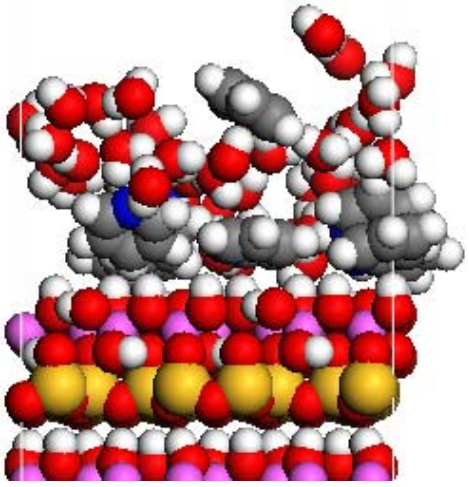

(b)

Figure 5.10 8 Pyridine Molecules and 40 Water Molecules on the Octahedral Surface (a) Before and (b) After 2,000 ps of MD Annealing

5.3.2 Water/Water Hydrogen Bonds

In order to discern whether water/water hydrogen bonds are the major driving force for the organic solvents adsorbed on the octahedral surface, the energies of the initial and final structures were compared and are listed in Table 5.1.

Table 5.1 VdW and Electrostatic Energies of the Initial and Final Structures of Systems shown in Figures 5.8-5.10

VdW	$E_{Initial}$ (kJ/mol)	E_{Final} (kJ/mol)	E_{Final}-$E_{Initial}$ (kJ/mol)
n-Heptane	335649±53	335685±48	36±71
Toluene	335711±18	335525±43	-185±47
Pyridine	335757±56	335715±23	-43±60
Electrostatic	$E_{Initial}$ (kJ/mol)	E_{Final} (kJ/mol)	E_{Final}-$E_{Initial}$ (kJ/mol)
n-Heptane	-555688±11	-555123±42	23±43
Toluene	-555340±68	-555020±100	319±121
Pyridine	-555264±101	-555208±5	52±101

Given the magnitudes of the vdW and electrostatic energy values, the calculated changes in the vdW and electrostatic energies basically are not considerable. In other words, the results shown in Figures 5.9 and 5.10 are not attributed to the decrease in energies of the systems.

Therefore, we speculated that it is the water/water hydrogen bonds that cause the water molecules desorbed from the octahedral surface. To quantify the amount of water/water hydrogen bonds, we determined the intermolecular O—H radial distribution function (i.e., $g_{OH}(r)$) of the systems shown in Table 5.1. In particular, we plotted the height of the peak appearing in the region below 2.5 Å

on the $g_{OH}(r)$ as a function of time (Figure 5.11). The peak(s) below the 2.5 Å region quantify the possibility of forming hydrogen bonds. For all cases, only one peak was found within this 2.5 Å in this region. Figure 5.11 indicates that the number of hydrogen bonds increases significantly as water desorbed from the surface. In the cases of *n*-heptane and pyridine, the number of water/water hydrogen bonds does not vary much over the course of the simulations. This may explain why *n*-heptane did not adsorb on the surface. However, it is not clear why the number of water/water hydrogen bonds does not vary. This may due to the fact that pyridine can form hydrogen bonds with water.

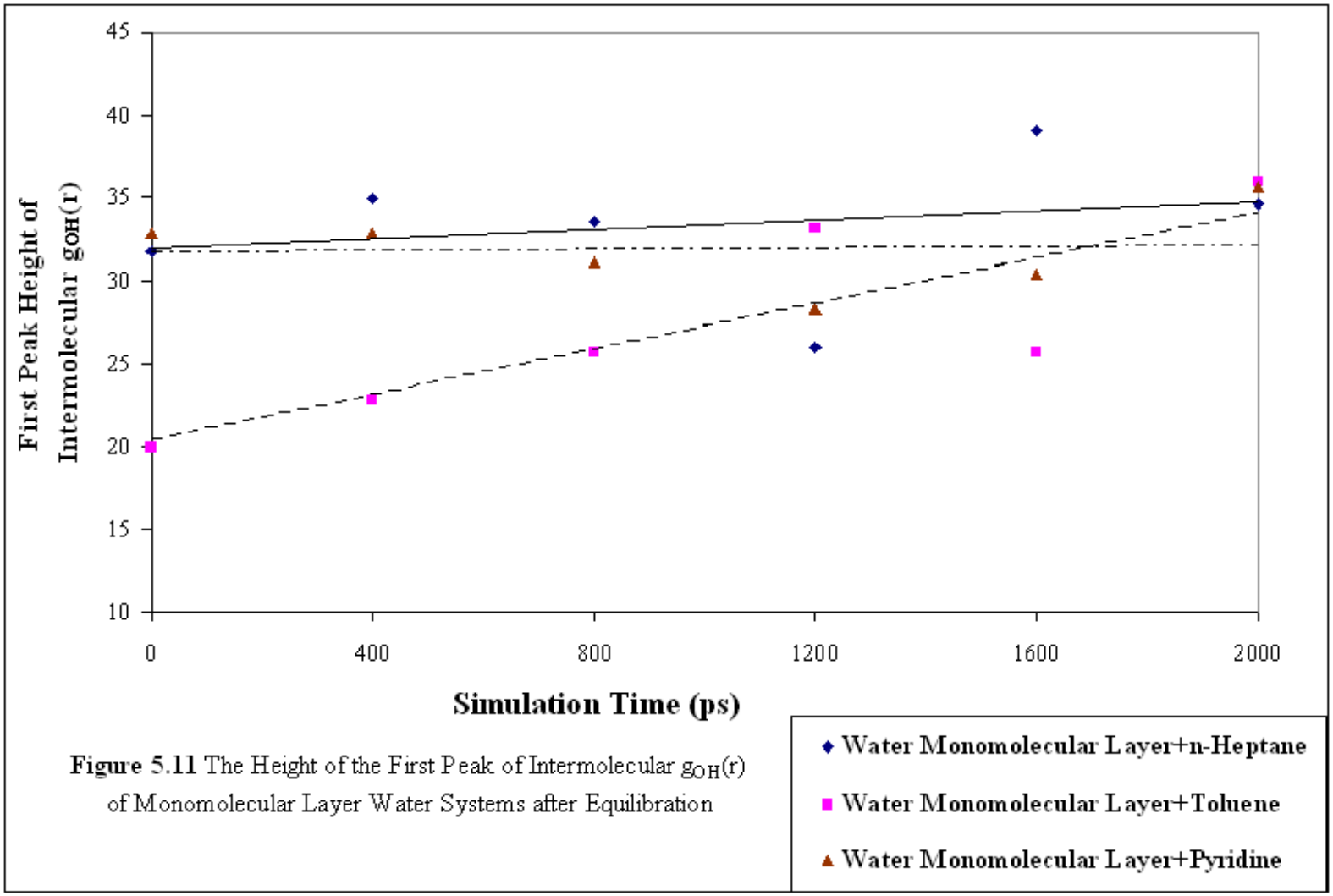

Figure 5.11 The Height of the First Peak of Intermolecular $g_{OH}(r)$ of Monomolecular Layer Water Systems after Equilibration

5.3.3 Wetting of Water Multi-molecular Layers in the Presence of Organic Molecules

Additional simulations with a thicker water layer (10.87 Å) were carried out, after 2,000 ps of MD annealing, none of *n*-heptane, toluene or pyridine molecules above the water layer (100 water molecules) showed any sign of moving closer to the octahedral surface as can be seen in Figures 5.12-5.14. These results are consistent with our expectation based upon the above discussion of water/water hydrogen bonds and the heat of immersion results discussed in Chapter 4.

The structures of these multi-molecular water layers were also investigated using $g_{OH}(r)$ (Figure 5.15). All three curves are similar indicating that the water structures are similar regardless of type of the organic molecules. However, toluene's peak is the highest indicating that there exist more water/water hydrogen bonds. This observation is consistent with the results shown in Figure 5.11 in which water tends to form more hydrogen bonds in the presence of toluene. Further investigation is needed.

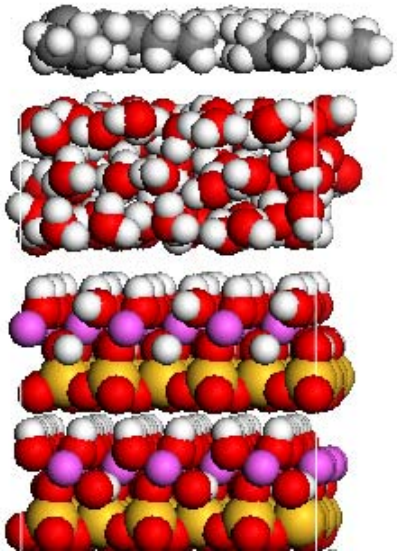

(a)

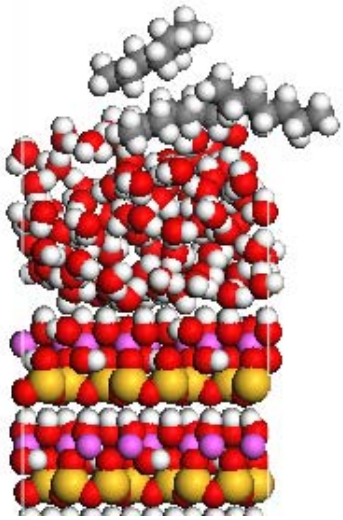

(b)

Figure 5.12 8 *n*-Heptane Molecules and 100 Water Molecules on the Octahedral Surface (a) Initial and (b) Structure after 2,000 ps of MD Annealing

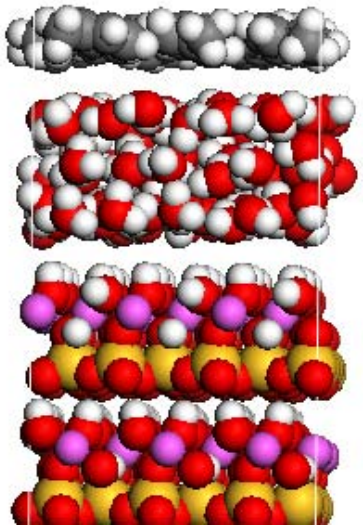

(a)

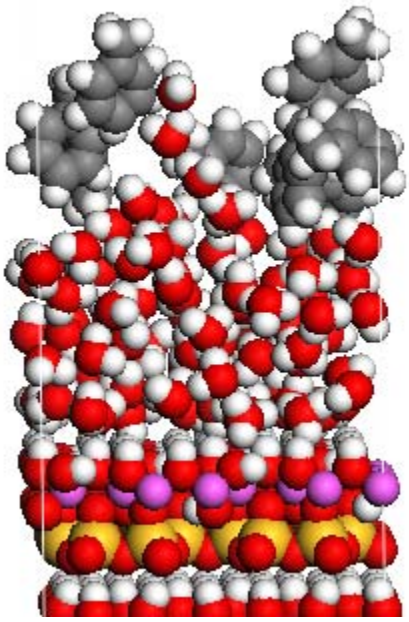

(b)

Figure 5.13 8 Toluene Molecules and 100 Water Molecules on the Octahedral Surface (a) Inital and (b) Structure after 2,000 ps of MD Annealing

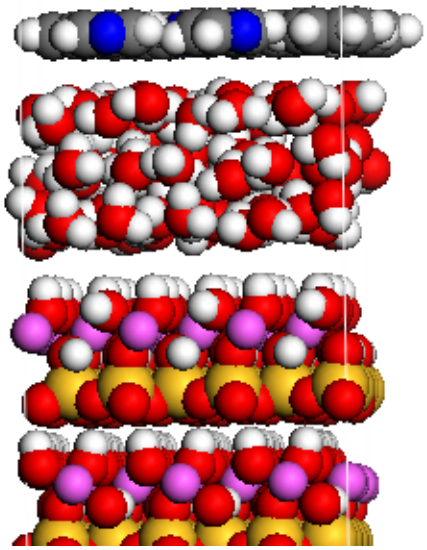

(a)

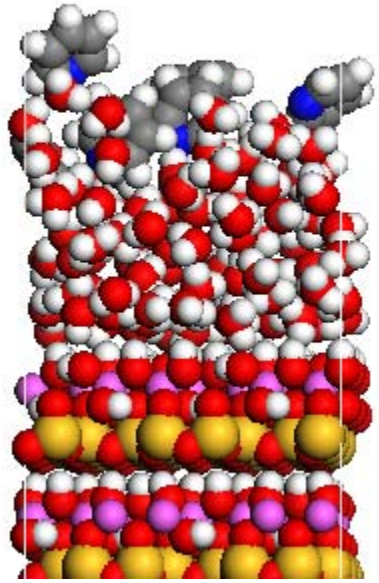

Figure 5.14 8 Pyridine Molecules and 100 Water Molecules on the Octahedral Surface (a) Initial and (b) Structure after 2,000 ps of MD Annealing

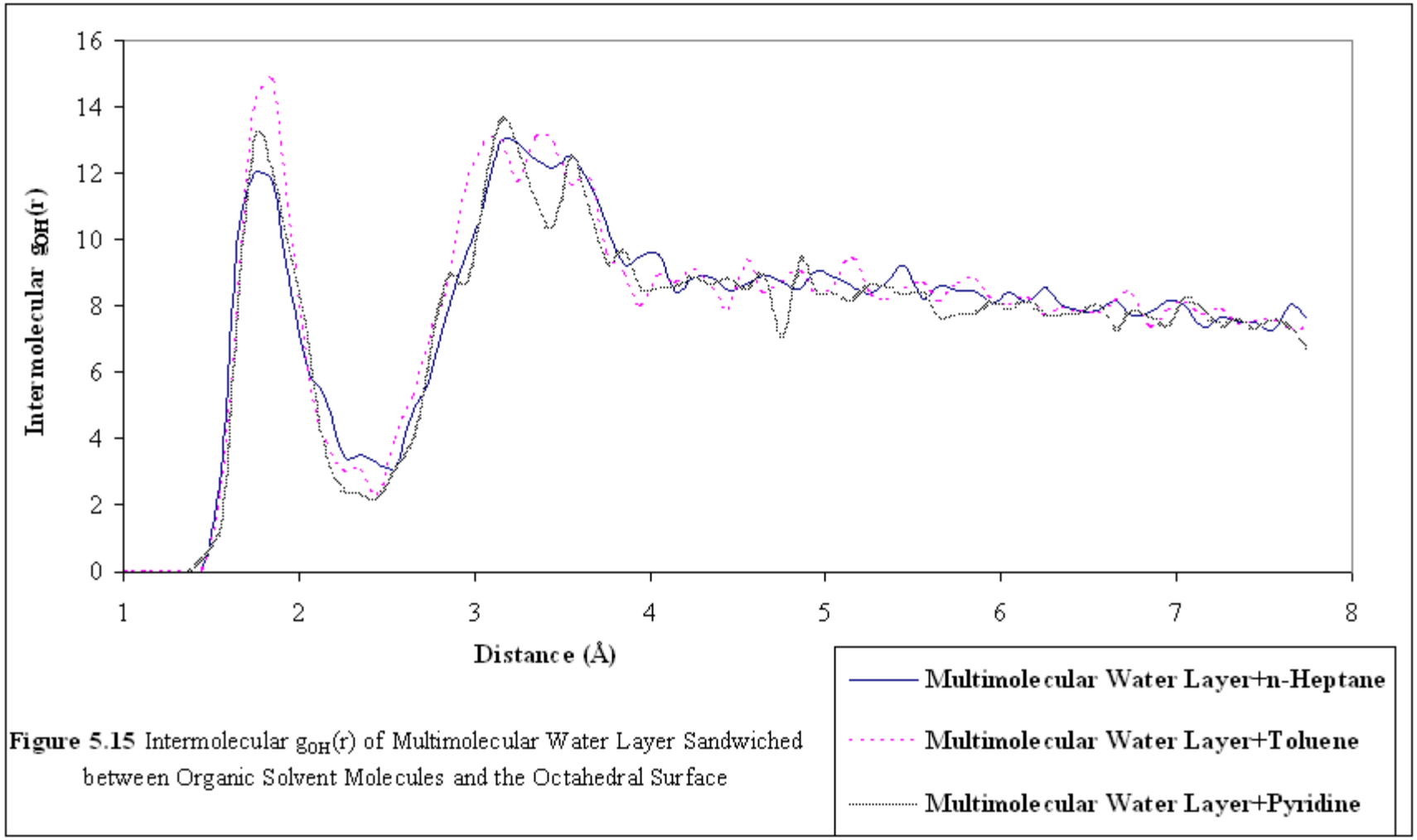

Figure 5.15 Intermolecular $g_{OH}(r)$ of Multimolecular Water Layer Sandwiched between Organic Solvent Molecules and the Octahedral Surface

5.4 Heat of Immersion of Monomolecular "Liquid" Layer

The simulation results of water monomolecular layer with the organic molecules are contradict to our expectation that water should exhibit the highest affinity as it shows the highest heat of immersion amongst the liquids studied in this work. This suggested that the concept of the heat of immersion may not be applicable to the current situation as there was only one molecular layer of water. This led to the calculations of the heats of immersion of single molecular layer of the "liquids".

Table 5.2 Calculated Heats of Immersion of Monomolecular Layers of *n*-Heptane, Toluene, Pyridine and Water on the Model Octahedral Surface at 298.13 K

Solvent type	$\Delta H_{imm,mono}$ (mJ/m^2)	Solvent type	$\Delta H_{imm,mono}$ (mJ/m^2)
n-Heptane	175±6	Pyridine	199±7
Toluene	195±3	Water	164±6

The above results are consistent with the simulation results shown in Figures 5.8-5.10. Nevertheless, comparison of the data shown in Table 5.2 and those in Table 4.3 indicates that ΔH_{imm} decreases as the thickness of the liquid layer decreases and that water exhibits the largest decrease. To understand why water exhibits the largest decrease in ΔH_{imm}, we compared the non-bonded energy terms of the systems used in Chapter 4 and those used in this section. It is worth pointing out here that the octahedral surfaces used in Chapter 4 and that used this chapter were the same, so the energy differences between the systems (octahedral surface + a "liquid" layer) are attributed to the differences in the solvent layer thickness. The

results are depicted in Figures 5.16 and 5.17. These two figures indicate that for all four liquids, the absolute values of electrostatic energies are higher than the vdW energies. This is consistent with our conclusions in Chapter 4 that the heat of immersion mainly depends on the electrostatic interaction. In fact, for all cases, the dispersion forces (i.e., E_{vdW}) act against wetting. The data also show that increasing the thickness of the organic solvent layer from a monomolecular layer to a multi-molecular layer, the vdW energies and long range electrostatic energies alters slightly for all organic solvents. This means that the heat of immersion is mainly dependent on the first molecular layer of these organic solvents, even in the case of pyridine which is a fairly polar molecule. Given the fact that the long range electrostatic interaction does not increase the heat of immersion from a monomolecular to multi-molecular layer, the substantial decrease in the case of water is attributed to the formation of more water/water hydrogen bonds in the multilayer environment (interlayer and interlayer hydrogen bonds). This is consistent with our observations that water/water hydrogen bonds could strongly affect liquid water behavior in section 5.3.

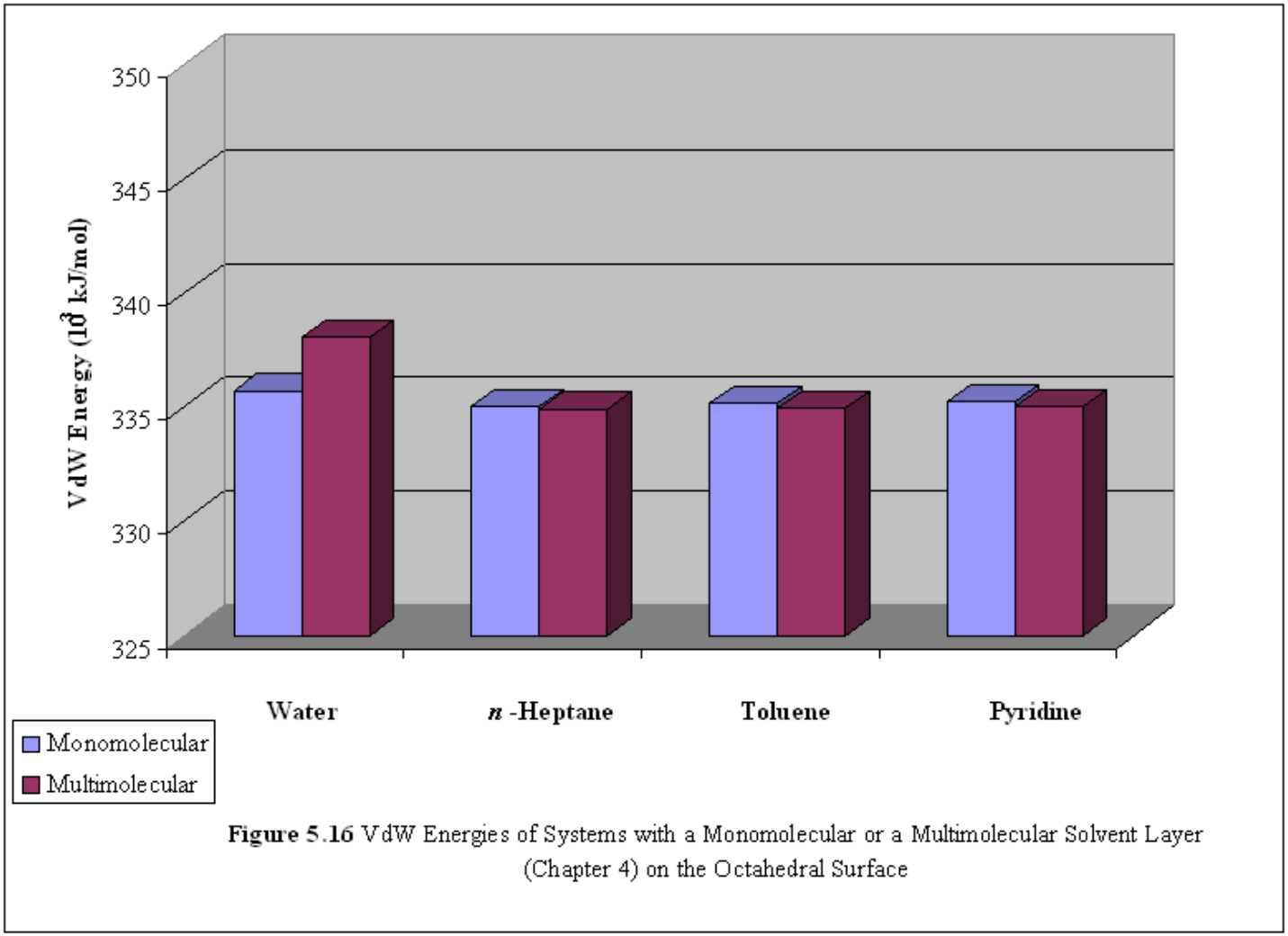

Figure 5.16 VdW Energies of Systems with a Monomolecular or a Multimolecular Solvent Layer (Chapter 4) on the Octahedral Surface

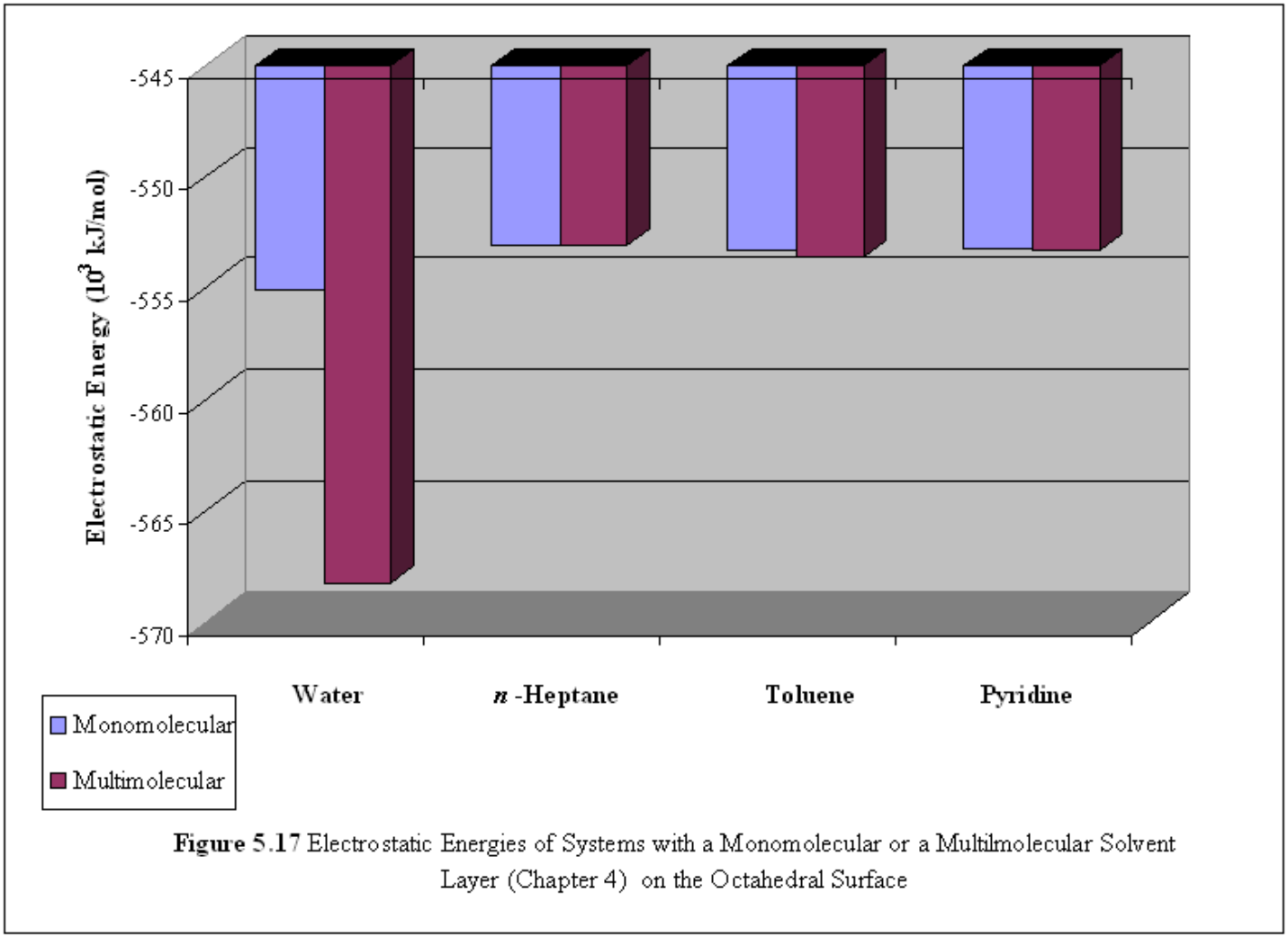

Figure 5.17 Electrostatic Energies of Systems with a Monomolecular or a Multilmolecular Solvent Layer (Chapter 4) on the Octahedral Surface

5.5 Summary

Under the vacuum, water molecules formed a more or less monomolecular layer on the octahedral surface of kaolinite but two molecular layers on the tetrahedral surface, indicating that water has a slightly higher affinity for the octahedral surface. This is consistent with the heats of immersion calculation of water on these two surfaces reported in Chapter 4.

The wettability simulations of a monomolecular layer of water in the presence of organic molecules indicated that water monomolecular layer is not stable on the octahedral surface. Heat of immersion calculations of the monomolecular layers of four liquids indicated that water exhibited the lowest affinity for the octahedral surface. Comparison of the results of the non-bonded energies of the systems using monomolecular and multi-molecular layers of water indicated that, the observed difference is mainly attributed to the hydrogen bonds. Hydrogen bonds in water are also the driving force for water desorption from the octahedral surface. However, when the thickness of the water layer is increased to ~11 Å (5-6 molecular layers), such a water layer was found quite stable, at least within the simulation time. This may due to water molecules can form interlayer and intralayer hydrogen bonds in the multi-molecular layers. In other words, the heat of immersion of water on the octahedral surface is controlled by multi-layers of water molecules while that of organic solvents only one or two molecular layers of molecules. This is simply due to the fact that organic solvents can not form hydrogen bonds with each other.

Based upon the results reported here, the hypothesis of the existence of a water layer on various mineral surfaces encountered in oil sands ores may be valid so long as the water layer is thicker than what we identified here. This is because molecules in bitumen tend to have higher molecular weight and to contain more unsaturation. Nevertheless, it is uncertain whether this layer of water would help or hinder the case of solvent for the extraction process.

5.6 References

Croteau, T., Bertram A. K., Patey, G. N. (2009) Simulation of Water Adsorption on Kaolinite under Atmospheric Conditions, *Journal of Physical Chemistry A*, 113, 7826-7833

Delville, A. (1995) Monte Carlo Simulation of Surface Hydration: An Application to Clay Wetting, *Journal of Physical Chemistry*, 99, 2033-2037

Roy, P. (2008) Course Notes of Chem 495: Molecular Dynamics and Its Applications, 2008, University of Alberta, AB

Sokolowski, S., Delville, A. (1993) Adsorption of Vapor at a Solid Interface: A Molecular Model of Surface Wetting, *Journal of Physical Chemistry*, 97, 6261-6271

Takei, T. and Chikazawa M. (1998) Origin of Differences in Heats of Immersion of Silicas in Water, *Journal of Colloid and Interface Science*, 208, 570-574

Van Duin, A. C. T., Larter, S. R. (2001) Molecular Dynamics Investigation into the Adsorption of Organic Compounds on Kaolinite Surfaces, *Organic Geochemistry*, 32, 143-150

Wang, J., Kalinichev, A. G., Kirkpatrick, R. J. (2009) Asymmetric Hydrogen Bonding and Orientational Ordering of Water at Hydrophobic and Hydrophilic Surfaces: A Comparison of Water/Vapor, Water/Talc, and Water/Mica Interfaces, *Journal of Physical Chemistry C*, 113, 11077-11085

Chapter 6

Conclusions and Future Work

6.1 Heat of Immersion

Molecular dynamics (MD) simulation and density functional theory (DFT) calculations are widely used to investigate structures, conformations and interactions of various molecular systems. In this work, MD and DFT calculations were used. DFT calculations were carried out to optimize the structure of four model inorganic surfaces including two sand surfaces and the octahedral and tetrahedral surfaces of kaolinite. MD simulations were then applied to calculate the heats of immersion of three organic solvents (*n*-heptane, toluene, and pyridine) and water on the aforementioned model surfaces. Heat of immersion can used to quantify the liquid of solvent for a surface. The results indicate that *n*-heptane has the weakest affinity for the clay model surfaces while water is strongest. Among the four model surfaces, kaolinite octahedral surface exhibited the strongest affinity for all liquids. Heat of immersion strongly depends on the electrostatic interaction. In the case of pyridine on the sand surface that cannot form hydrogen bonds (HWOH), interfacial hydrogen bonds seem to increase the heat of immersion. In the simulations of water on the octahedral surface, it was found that water/water hydrogen bonds contribute significantly to the calculated heat of immersion. It is expected to be true for the sand surfaces although comparable simulations (more molecular layer simulations) were not carried out.

The heat of immersion calculations alone indicated that there could be a layer of water on the model mineral surfaces. The existence of such a layer of water may have influence on the choice of solvent for a solvent extraction process.

6.2 Wettability of Water on Selected Clay Surfaces

Only kaolinite basal surfaces were employed in our calculations, because clays are considered more problematic in the current oil sands extraction process. From the trajectories of the simulation, water molecules formed a more or less monomolecular layer on the octahedral surface while two molecular layers on the tetrahedral surface. This indicated that the octahedral surface has stronger affinity for water than the tetrahedral surface. This is consistent with the heats of immersion results reported in Chapter 4.

Wettability simulations of water layer on the octahedral surface in the presence of an organic layer (*n*-heptane or toluene or pyridine) above the water layer were also conducted. It is shown that the monolayer of water molecules was not stable on the octahedral surface, especially in the presence of toluene and pyridine. The heat of immersion calculations of monomolecular "liquid" layer indicated that water monomolecular layer exhibited the lowest affinity for the octahedral surface. The non-bonded energies of the systems with monomolecular and multi-molecular solvent layers were compared. In all cases, electrostatic forces are in favor of wetting of liquids. Increasing the thickness of the organic solvent layer from monomolecular layer to multi-molecular layers, the vdW energies and electrostatic energies altered slightly. However, this is not the case

for water. It was found that the decrease in the electrostatic energy in the case of multimolecular layer water was attributed to water/water hydrogen bonds in the water layer. In other words, heat of immersion depends on more than one or two molecular layers of water, while for organic solvents, they are controlled by a couple of molecular layers adjacent on the interface. Also such water/water hydrogen bonds cause monomolecular layer of water molecules desorbed from the octahedral surface. Nonetheless, it was found that 5 or 6 molecular (i.e. ~10 Å) layers of water was fairly stable, at least over a simulation time of 2,000 ps. This is also attributed to the fact that there exist a considerable number of interlayer and intralayer hydrogen bonds.

The hypothesis of a thin layer of water existing on the mineral surfaces seems to be plausible so long as the water layer is of multi-molecular layers thick. Based upon our simulation results of *n*-heptane, toluene and pyridine, 5 or 6 molecular layers of water could be stable on the octahedral surface. However, in the presence of molecules encountered in bitumen such as asphaltenes, more molecular layers of water are expected to stabilize the water layer.

6.3 Future Works

Wettability of water layer on tetrahedral surface and silica model surfaces should also be conducted in the future. A systematic study of the stability of water layer sandwiched between various organic molecules and mineral surfaces should also be carried out. Model asphaltene molecules and molecules with different functional groups should be used in such simulations.